JAERI-Data/Code
96-005

EXPERIMENTS ON IRON SHIELD TRANSMISSION OF QUASI-MONOENERGETIC NEUTRONS GENERATED BY 43-AND 68-MeV PROTONS VIA THE ^{7}Li(p,n) REACTION

March 1996

Hiroshi NAKASHIMA, Noriaki NAKAO[*1], Shun-ichi TANAKA
Takashi NAKAMURA[*2], Kazuo SHIN[*3], Susumu TANAKA
Shin-ichiro MEIGO, Yoshihiro NAKANE, Hiroshi TAKADA
Yukio SAKAMOTO and Mamoru BABA[*4]

日本原子力研究所
Japan Atomic Energy Research Institute

本レポートは，日本原子力研究所が不定期に公刊している研究報告書です。
入手の問合わせは，日本原子力研究所技術情報部情報資料課（〒319-11 茨城県那珂郡東海村）あて，お申し越しください。なお，このほかに財団法人原子力弘済会資料センター（〒319-11 茨城県那珂郡東海村日本原子力研究所内）で複写による実費頒布をおこなっております。

This report is issued irregularly.
Inquiries about availability of the reports should be addressed to Information Division, Department of Technical Information, Japan Atomic Energy Research Institute, Tokai-mura, Naka-gun, Ibaraki-ken 319-11, Japan.

編集兼発行　日本原子力研究所
印　　刷　㈱原子力資料サービス

JAERI－Data/Code 96－005

Experiments on Iron Shield Transmission of Quasi-monoenergetic Neutrons Generated by 43- and 68-MeV Protons via the ^{7}Li(p,n) Reaction

Hiroshi NAKASHIMA, Noriaki NAKAO*1, Shun-ichi TANAKA+ , Takashi NAKAMURA*2
Kazuo SHIN*3, Susumu TANAKA++, Shin-ichiro MEIGO, Yoshihiro NAKANE
Hiroshi TAKADA, Yukio SAKAMOTO and Mamoru BABA*4

Department of Reactor Engineering
Tokai Research Establishment
Japan Atomic Energy Research Institute
Tokai-mura, Naka-gun, Ibaraki-ken

(Received February 7, 1996)

In order to provide benchmark data of neutrons transmitted through iron shields in the intermediate-energy region, spatial distributions of neutron energy spectra and reaction rates behind and inside the iron shields of thickness up to 130 cm were measured for 43- and 68-MeVp-^{7}Li neutrons using a quasi-monoenergetic neutron beam source at the 90-MV AVF cyclotron facility of the TLARA facility in JAERI. The measured data by five kinds of detectors: the BC501A detector, the Bonner ball counter, ^{238}U and ^{232}Th fission counters, ^{7}LiF and ^{nat}LiF TLDs and solid state nuclear track detector, are numerically provided in this report in the energy region between 10^{-4} eV and the energy of peak neutrons generated by the ^{7}Li(p,n) reaction.

Keywords: Iron, Benchmark Experiment, Transmission, Quasi-monoenergetic Neutron Beam Source, Intermediate Energy, Neutron Spectrum, Neutron Reaction Rate, Neutron Dose Equivalent

---

This research report is the result of the joint study with University of Tokyo, Tohoku University and Kyoto University.

+ Office of Planning
++ Advanced Radiation Technology Center, Takasaki Radiation Chemistry Research Establishment
*1 University of Tokyo, Institute for Nuclear Study
*2 Tohoku University, Cyclotron and Radioisotope Center
*3 Kyoto University
*4 Tohoku University

JAERI－Data/Code 96－005

43及び68MeV陽子により発生する準単色中性子の鉄遮蔽体透過実験

日本原子力研究所東海研究所原子炉工学部

中島　宏・中尾　徳晶[*1]・田中　俊一[+]・中村　尚司[*2]

秦　和夫[*3]・田中　進[++]・明午伸一郎・中根　佳弘

高田　弘・坂本　幸夫・馬場　譲[*4]

（1996年2月7日受理）

中間エネルギー領域中性子の鉄遮蔽体透過に関するベンチマークデータを取得するために，原研高崎研の90MV－AVFサイクロトロンの単色中性子発生装置を用いて，43及び68MeV陽子により薄い^{7}Liターゲットから発生するビーム状準単色中性子が，0cmから130cmの厚さの鉄遮蔽体を透過したときの，遮蔽体後面における中性子エネルギースペクトル及び遮蔽体内部の中性子反応率の分布を測定した。本報告書には，5種類の検出器，即ちBC501Aシンチレーション検出器，ボナーボール検出器，^{238}U及び^{232}Th 核分裂計数管，^{7}LiF及び^{nat}LiF TLD，固体飛跡検出器を用いて測定した。^{7}Li(p,n)反応による中性子ピークエネルギーから10^{-4}evに至るエネルギー範囲に対する測定値の数値データが記載されている。

本報は，東京大学，東北大学及び京都大学との共同研究の成果である。

東海研究所：〒319-11　茨城県那珂郡東海村白方白根２－４

[+] 企画室

[++] 放射線高度利用センター

[*1] 東京大学原子核研究所

[*2] 東北大学サイクロトロンＲＩセンター

[*3] 京都大学

[*4] 東北大学

Contents

目　　次

1. INTRODUCTION

Intermediate- and high-energy accelerators are recently planed and constructed for utilization in various fields: physical, engineering and medical use. With increasing the energy and intensity of accelerated particles, the neutrons generated by the particles have strong penetrability and the facility requires more massive shields. In the facilities sophisticated shielding designs are required to keep regulations for the dose limit and to prevent from activations of devices as well as to save the building cost. Several codes and code systems have been developed to achieve the suitable shielding design.[1,2,3] The codes are, however, designed for the particle transport calculation in the energy region above 100 MeV. On the other hand, the neutron transport calculation in intermediate-energy region between 20 and 100 MeV is the most crucial part on accelerator shielding, because nuclear reactions are complex. Therefore, the validity of the calculation methods should be confirmed by benchmark experimental data on the neutron transmitted through the bulk shields in the energy region.

A few neutron spectra behind the bulk shield have been measured for neutron source in the intermediate energy region.[4,5,6,7] Shin and Uwamino's measurements have used source neutrons of broad energy spectra generated via the C(p,n) reaction by 52-MeV proton and the Cu(p,n) reaction by 65-MeV proton. Ishikawa et al. have measured the transmitted spectra along the beam axis for quasi-monoenergetic source neutrons generated via the ^{7}Li(p,n) reaction by 25- and 35-MeV protons.

A quasi-monoenergetic neutron field using the ^{7}Li(p,n) reaction was recently established at the 90-MV AVF cyclotron facility of the TIARA (Takasaki Ion Accelerator for Advanced Radiation Application) facility in JAERI (Japan Atomic Energy Research Institute), where neutron beam is served for shielding experiments. In the neutron field we can study the elastic and inelastic scattering reactions respectively by using the quasi-monoenergetic neutrons, and investigate the angular distribution of the scattering reaction by using neutron beam and measuring spacial neutron distribution transmitted through shields.

In this study, iron was chosen as a shielding material, because iron was often used for massive shields around beam dumps and targets, and monogenetic material was effective for investigating the nuclear reaction. The spatial and energy distributions of neutrons transmitted through iron shields were measured using source neutron beam generated via the ^{7}Li(p,n) reaction by 43- and 68-MeV protons. The objective is to provide benchmark data of neutrons

transmitted through iron shields for investigating the accuracy of calculation codes and cross section data libraries.

2. EXPERIMENT

2.1 TIARA facility and experimental set up

The experiment was carried out at the AVF cyclotron facility of the Takasaki site at JAERI, which had a neutron beam course, LC-course, arranged for the neutron shielding and cross section experiments. The cross sectional view is shown in Fig.1. The neutron generated at the accelerator room passed to the experimental room (the 3rd light-ion room) through a 10.9-cm-diam. x 225-cm-long iron collimator embedded in a concrete wall. The collimator is used as a rotary beam shutter, through which the neutron beam was injected into the shield when the shutter was open, as shown in Fig.1. The iron shield of 10 to 130 cm thickness was assembled by 120 cm x 120 cm by 10-cm-thick slabs and was fixed on a movable stand to set in contact with the collimator exit located at 4 m from the neutron target. The additional collimator shown in Fig.2 were used only for off-center measurements with thinner shield: 10-, 20- and 40-cm-thick iron, in order to depress the contribution of neutrons leaked through filler of iron ball and iron sand or rotary shutter of iron and polyethylene which includes low density space of air gap in the concrete wall. The additional iron collimator was composed of 120 cm x 120 cm slab of 10 cm thickness with a 10.9-cm-diam. cylindrical hole equal to that of the rotary shutter collimator. The combination of the shield and additional collimator are given in Table 1, and the atomic compositions of iron shield, additional iron collimator and the concrete wall are tabulated in Table 2.

2.2 Neutron sources

The source neutrons were generated by 43- and 68-MeV protons bombarding 3.6-mm-thick and 5.2-mm-thick, 99.9 % enriched ^{7}Li targets, respectively, in the target chamber in the accelerator room. The protons penetrated the target with the 2-MeV energy loss were bent down toward the beam dump by the clearing magnet. The beam dump consists of 30 cm x 30 cm x 50 cm hole surrounded by iron in the concrete wall as shown in Fig.1. The neutrons produced in the forward angle can reach the experimental room through the collimator.

The spectra of quasi-monoenergetic neutron source were measured with a BC501A liquid scintillation counter using the time of flight (TOF) method. The block diagram of the measuring electronic circuit is shown in Fig.3 for the TOF measurement. The detector was placed about 14 m away from the target, and the repetition periods of the proton beam from the cyclotron:

15.460 and 18.919 MHz, were extended to one seventh by beam choppers in order to measure the neutron spectra down to a few MeV. The efficiency of the scintillator for the TOF measurement was obtained from the measured response matrix[8]. The measured source neutron energy spectra are shown in Fig. 4 and tabulated in Tables 3 and 4.

The absolute flux of source neutrons in the monoenergetic peak per proton beam charge (μC) has been measured by a proton-recoil-counter-telescope (PRT) set at the position of 5.54 m from the target.[9] The neutron fluxes in the monoenergetic peak measured by the TOF method were normalized by the absolute value measured by PRT.

During the experiment, the number of protons incident on the Faraday cup was measured using the current integrator connected to the Faraday cup in the beam dump. The range of proton currents in this experiment was 0.5 nA to 3 mA. The counts of two neutron fluence monitors (^{238}U and ^{232}Th fission counters) placed near the target were normalized to the absolute peak neutron flux through the amount of total charges of proton beam, and were used for calculating the real total proton charges even in the low beam current runs in order to reduce the uncertainty of dark current on the Faraday cup.

2.3 Detectors and data analyses for shielding experiment

For the shielding experiment five kinds of detectors were applied for the measurement of neutron spectra and reaction rates behind and inside the iron shields. The detectors used for the iron shielding experiment and the measured positions are summarized in Table.1.

2.3.1 BC501A liquid scintillation counter

One of the neutron spectrometry in the shielding experiment was performed with the 12.7-cm-diam. x 12.7-cm-long BC501A organic liquid scintillator (Bicron Co. Ltd.) coupled to a R4143 photomultiplier (Hamamatsu Photonics. Co. Ltd.). The block diagram of the measuring electronic circuit for the shielding experiment is also shown in Fig.3. The rise-time pulses which distinguished between neutron-event and photon-event were supplied by the rise-rime-to-height converter (OHYO KOKEN KOGYO Co., Ltd.). In the shielding experiment, the two pulses of pulse-height and rise-time were recorded in event-by-event mode. These data were taken by the ND9900 MPA 8/16 (CAMBERRA Co. Ltd.) and the VAX STATION 3100 (DEC Co. Ltd.), then recorded in a hard disk.

The event-by-event data measured with BC501A were converted to two dimensional distribution of pulse-height and rise-time, and the pulse-height distributions induced by neutrons were selected by eliminating the γ-ray pulses. Then they were converted into the neutron energy spectra using the FERDOU unfolding code[10] and the measured response matrix[8]. The energy calibration of the light output pulses was performed using the Compton edge of 4.43-MeV γ-rays from a ^{241}Am-Be source and the recoiled proton edge of 40- or 65-MeV monoenergetic neutron peak of 43- or 68-MeV p-Li reaction fitted to the calibration values from Ref.[8], and using the zero point with a Research Pulser. The dead time correction of the data taking system was done from the difference of the number counted in the scaler and the number of events which were recorded in the hard disk. Finally the absolute values of the transmitted spectra are presented as the flux per proton beam charge (μC) which can be estimated from the fluence monitor counts.

2.3.2 Bonner ball counter

Multi-moderator spectrometer, Bonner ball, with four spherical polyethylene moderators of 1.5, 3.0, 5.0 and 9.0 cm thicknesses and without moderator was also used for the shielding experiment. The thermal neutron detector inserted in the center of the moderator is a 5.08-cm-diam. spherical proportional counter, made by LND Inc., filled with 10 atm (at 22 °) ^{3}He gas. The pulse height spectra for five different moderators of the Bonner ball counter were recorded.

The pulse height data measured with the Bonner ball counter were summed up to get counts above the γ-ray discrimination level. These five counts measured for five moderators were unfolded with the SAND-2 code[11] and the response matrix given by Uwamino et al[12]. The response matrix is shown in Fig. 5 and given in Table 5. Initial guess spectra used in unfolding were obtained from the MORSE[13] calculations with the HILO86 group cross section set[14] at each measured position. We then obtained the spectra of neutrons in the energy range from 10^{-4} eV to the peak energy.

2.3.3 Fission counters

^{238}U and ^{232}Th fission counters (Centronic FC480/1000) with a 10.1-cm-long x 3.81-cm-diam. active volume were used for measuring neutron reaction rates behind the iron shield.

The absolute efficiencies were calibrated by the ^{252}Cf spontaneous fission neutron source of Facility of Radiation Standard (FRS)[15] of JAERI. The facility is the second standard field of neutron. The neutron source had an intensity of 1.218 x 10^8 n/sec with the uncertainty of ±3%. The measured efficiencies are 1.05 x 10^3 and 9.86 x 10^2 barn/cm^2/counts (±4 and 3.4%), respectively. The fission cross sections of ^{238}U and ^{232}Th have been evaluated up to 20 MeV in JENDL－3[16], measured by Lisowski et al.[17,18] in the energy region between 20 and 400 MeV and calculated using the HETC code above 400 MeV. The cross sections are shown in Fig. 6 and the group cross section data are given in Table 6.

2.3.4 Thermoluminescent dosimeter (TLD)

Neutron reaction rates were measured on the axis of the beam in the iron shield using ^{7}LiF and ^{nat}Li TLDs (Harshaw Co. Ltd.) of 1 x 1 x 6 mm^3. Thermoluminescence was read out by a TLD reader (Harshaw 2000), and converted to the absolute dose in TLDs using a calibration factor determined with ^{60}Co γ－rays of FRS within the uncertainty less than 3 %. The neutron energy responses were calculated by a code developed by Hashikura et al. which was based on a KERMA calculation[19]. The calculated neutron energy responses are shown in Fig. 7 and tabulated in Table 7.

2.3.5 Solid state nuclear track detector (SSNTD)

The neutron reaction rates in the shield were also measured using a solid state nuclear track detector: Types TS－16N resin manufactured by Fukuvi Chemical Industry Co. Ltd. from a monomer (TS－16N) made by Tokuyama Soda Ltd. The composition of the detector is the same as that of CR－39 (Allyl diglycol carbonate). The detector is a rectangular solid of 10 x 5 x 1 mm^3 attached with a polyethylene radiator of 1 mm thick. After the exposed detectors were etched chemically, the etch pits on the detectors were counted through the optical microscope of 400 times magnifications. The neutron response was calculated by a Monte Carlo code system: SSNRES[20], based on the SCINFUL code[21]. The calculated neutron response is shown in Fig. 8 and given in Table 8.

3. RESULTS

3.1 Neutron spectra in the energy region above a few MeV measured by the BC501A detector

Neutron spectra in the energy region above a few MeV were measured just behind the iron shield on the beam axis and at the off-center positions of 20 and 40 cm from the beam axis as tabulated in Table 1 using the BC501A detector. Figure 9 shows the measured neutron energy spectra behind various thickness of iron up to 100 cm on the beam axis for 43-MeV p-Li neutrons. The errors of the measurement in the figure include only errors of spectrum unfolding and counting statistics in the measurement, neglecting that the source neutron flux has errors of PRT(3-5%), conversion factor of fluence monitor to total charges of proton beam (3%), neutron penetration factor through objects on the beam line (3%) and the fluence monitor counting statistics (less than 1%). The measured neutron spectra at the positions of 20 and 40 cm from the beam axis behind 0-, 10-, 20- and 40-cm thick shields are shown in Figs. 10 through 13 for 43-MeV p-Li neutrons, respectively. The measured neutron spectra for 68-MeV p-Li neutrons are also shown in Figs. 14 through 17 behind the iron shield of thickness up to 130 cm on the beam axis and at the positions of 20 and 40 cm from the beam axis. The measured neutron spectra are also tabulated in Tables 9 through 20.

3.2 Neutron reaction rates and spectra in the energy region up to a few MeV measured by the Bonner ball counter

Neutron reaction rates behind the iron shields up to 100 cm thick on the beam axis were measured using the Bonner ball counter with four spherical polyethylene moderators of 1.5, 3.0, 5.0 and 9.0 cm thicknesses and without moderator as given in Tables 21 and 22. Neutron spectra obtained from the reaction rates using the SAND-2 unfolding code and the calculated response matrix are shown in Figs. 18 and 19 for 43- and 68-MeV p-Li neutrons, and the numerical data are given in Tables 23 ad 24. The experimental errors of the Bonner ball counter could not be obtained since the SAND-2 unfolding code can not give them.

3.3 Neutron reaction rates measured by fission counters, TLDs and SSNTD

Fission reaction rates were measured behind the shields of various thicknesses on the beam axis and at the position of 20 cm from the beam axis using ^{238}U and ^{232}Th fission counters, as

shown in Figs. 20 and 21, and given in Tables 25 and 26 for 43- and 68-MeV p-Li neutrons. The uncertainties of the measured data shown in the figures include the counting statistics of the fission counters and neutron intensity monitor. The reaction rates indicate the integrated neutron flux in the energy region above the threshold energy of the fission reactions: about 1 MeV.

In Table 27 the differences of neutron reaction rates measured by ^{7}LiF and ^{nat}LiF TLDs in the iron shield are given for 43- and 68-MeV p-Li neutrons. The differences are dominated by the neutron in the energy region up to 1 MeV as shown in Fig. 7. The errors of the measurements are the counting statistics of each detector and neutron intensity monitor.

The measured neutron reaction rates in the iron shield are shown in Fig. 22 and given in Table 28 using SSNTD for 43- and 68-MeV p-Li neutrons. As shown in Fig. 8, the efficiency of the detector is dominated by the neutron in the energy region up to about 10 MeV. The uncertainties of the measurements include the counting statistics of etch pits and neutron intensity monitor.

The combination of the reaction rates measurements covers the whole energy region up to the energy of peak neutrons produced by the neutron source, and the results of these measurements are effective to confirm the integrated neutron flux in each energy region.

3.4 Neutron dose equivalent

The neutron reaction rates measured by a rem counter, made by the Fuji Co. Ltd. are tabulated in Table 29 as a reference of neutron dose equivalents. Neutron dose equivalents were also estimated from the neutron spectra above 10 MeV measured by the BC501A detector and the neutron spectra up to 10 MeV by the Bonner ball counter by multiplying the ICRP21 neutron-flux-to-dose conversion factor[22], as given in Table 30. The neutron dose equivalents are compared with the neutron reaction rates measured by the rem counter in Fig. 23. The measured reaction rates by the rem counter are lower than the evaluated values behind the iron shield of 20 cm thickness, while higher behind the iron shield of 100 cm thickness. The discrepancy is caused by the response function of the rem counter. The detector does not have the same response function as the dose conversion factor in the energy regions above 20 MeV and between a few hundred keV and a few keV.

4. SUMMARY

The spatial distributions of neutron energy spectra and reaction rates behind and inside the iron shields up to 130 cm were measured for 43- and 68-MeV p-Li neutrons, which cover the energy region between 10^{-4} eV and the energy of peak neutrons generated via the ^{7}Li(p,n) reaction using five kinds of detectors: the BC501A detector, the Bonner ball counter, ^{238}U and ^{232}Th fission counters, ^{7}LiF and ^{nat}LiF TLDs and SSNTD.

The data measured absolutely were tabulated in this report in order to estimate the accuracy of the calculation code and cross section data set in the intermediate energy region. As shown in figures in this report, the energy spectra measured using the quasi-monoenergetic neutron source give useful information for investigating the elastic and inelastic scattering reactions respectively, and the spatial distributions behind the iron shields obtained using neutron beam are valuable for studying the angular distribution of the scattering reaction. The measurement in the wide energy range provided the neutron dose equivalents behind the iron shields due to the intermediate-energy neutrons.

ACKNOWLEDGMENTS

We wish to thank the operation staff of TIARA for the cyclotron operation. This work has been supported by the Universities-JAERI Collaborative Project Research Program.

4. SUMMARY

The spatial distributions of neutron energy spectra and reaction rates behind and inside the iron shields up to 130 cm were measured for 43- and 68-MeV p-Li neutrons, which cover the energy region between 10^{-4} eV and the energy of peak neutrons generated via the ^{7}Li(p,n) reaction using five kinds of detectors: the BC501A detector, the Bonner ball counter, ^{238}U and ^{232}Th fission counters, ^{7}LiF and ^{nat}LiF TLDs and SSNTD.

The data measured absolutely were tabulated in this report in order to estimate the accuracy of the calculation code and cross section data set in the intermediate energy region. As shown in figures in this report, the energy spectra measured using the quasi-monoenergetic neutron source give useful information for investigating the elastic and inelastic scattering reactions respectively, and the spatial distributions behind the iron shields obtained using neutron beam are valuable for studying the angular distribution of the scattering reaction. The measurement in the wide energy range provided the neutron dose equivalents behind the iron shields due to the intermediate-energy neutrons.

ACKNOWLEDGMENTS

We wish to thank the operation staff of TIARA for the cyclotron operation. This work has been supported by the Universities-JAERI Collaborative Project Research Program.

REFERENCES

1. Cloth P., Filges D., Neef R.D., Sterzenbach G, Reul Ch., T. W. Armstrong T.W., Colborn B.L., B. Anders B. and Bruckmann H.: FA－IRE－E AN/12/88, "HERMES A Monte Carlo Program System for Beam－Materials Interaction Studies" (1988).
2. Prael R.E. and Lichtenstein H.: LA－UR－89－3014, "USER GUIDE TO LCS: THE LAHET CODE SYSTEM" (1989).
3. Nakahara Y. and Tsutsu T.: JAERI－M 82－198, "NMTC/JAERI A Simulation Code System for High Energy Nuclear Reactions and Nucleon－Meson Transport Processes" (1982).
4. Shin K., Uwamino Y., Yoshida M., Hyodo T. and Nakamura T.: "Penetration of Secondary Neutrons and Photons from a Graphite Assembly Exposed to 52－MeV Protons", Nucl. Sci. Eng., 71, 294 (1979).
5. Uwamino Y., Nakamura T. and Shin K.: "Penetration Through Shielding Materials of Secondary Neutrons and Photons Generated by 52－MeV Protons", Nucl. Sci. Eng., 80, 360 (1982).
6. Shin K., Ishii Y., Miyahara K., Uwamino Y., Sakai H. and Nurata T.: "Transmission of Intermediate－Energy Neutrons and Associated Gamma Rays Through IRON, Lead, Graphite and Concrete Shields", Nucl. Sci. Eng., 109, 380 (1991).
7. Ishikawa T., Miyama Y. and Nakamura T.: "Neutron Penetration Through Iron and Concrete Shields with the Use of 22.0－ and 32.5－MeV Quasi－Monoenergetic Sources", Nucl. Sci. Eng., 116, 278 (1994).
8. Baba M., Kiyosumi T., Iwasaki T., Yoshioka M., Matsuyama S., Hirakawa N., Nakamura T., Tanaka Su., Tanaka R., Tanaka Sh., Nakashima H. and Meigo S.: JAERI－M 94－019, p.200, "Characterization and Application of 20－90 MeV ^{7}Li(p,n) Neutron Source at TIARA" (1994).
9. Shin K., Uwamino Y. and Hyodo T.: "Propagation of Errors from Response Functions to Unfolded Spectrum", Nucl. Technol., 53, 78 (1981).
10. Nakao N., Nakamura T., Baba M., Uwamino Y., Nakanishi N., Nakashima H. and Tanaka S.: "Measurements of Response Function of Organic Liquid Scintillator for Neutron Energy Range up to 135 MeV", Nucl. Instrum. Methods, A362, 454 (1995).
11. Mcelroy W.N., Berg S., Crokett T. and Hawkins R.G.: AFWL－TR－67－41, Vols. 1 through 4, Air Force Weapons Laboratory, "A Computer Automated Iterative Methods for Neutron Flux Spectra Determination by Foil Activation" (1967).
12. Uwamino Y., Nakamura T. and Hara A.: "Two Types of Multi－Moderator Neutron Spectrometers: Gamma－Ray Insensitive Type and High－Efficiency Type", Nucl. Instrum. Methods in Phys. Res., A239, 299 (1985).
13. Straker E.A., tevens P.N., Irving D.C. and Cain V.R.: ORNL－4585, "The MORSE Code －A Multi－Group Neutron and Gamma－Ray Monte Carlo Transport Code" (1970).
14. Alsmiller R.G. Jr., Barnes J.M. and Drischler J.D.: ORNL/TM－9801, "Neutron－Photon

Multigroup Cross Sections for Neutron Energies <400 MeV (Revision 1)" (1986).

15. Yoshizawa M.: private communication.
16. Shibata K. et al.: JAERI 1319, "Japanese Evaluated Nuclear Data Library, Version－3 －JENDL－3－" (1990).
17. Lisowski P.W. et al.: "Neutron Induced Fission Cross Section Rates for ^{232}Th, $^{235, 238}$U, ^{237}Np and ^{239}Pu from 1 to 400 MeV", Proc. Int. Conf. Nuclear Data for Sci. and Technol., Mito, Japan, p.97－99 (1988).
18. Lisowski P.W. et al.: "Fission Cross Sections in the Intermediate Energy Region", Proc. Spec. Meet. on Neutron Cross Section Standards for the Energy Region above 20 MeV, Uppsala, Sweden, 21－23 May, 1991, p.177－186 (1991).
19. Hashikura H., Haikawa K., Tanaka S. and Kondo K.: "Calculation of Neutron Response of Thermoluminescent Dosimeters", J. Faculty of Eng., Univ. of Tokyo, 39(1), 7 (1987).
20. Nakane Y.: private communication.
21. Dickens J.K.: ORNL－6463, "SCINFUL: A Monte Carlo Based Computer Program to Determine a Scintillator Full Energy Response to Neutron Detection for En Between 0.1 and 80 MeV: Program Development and Comparisons of Program Predictions with Experimental Data" (1988).
22. "Data for Use in Protection Against External Radiation", Ann. ICRP, 17, 2/3 (1987).

Table 1 Dimensions of the iron shield assembly and additional collimator, and detector positions.

Ep[a] (MeV)	Shield thickness (cm)	Collimator length (cm)	Peak flux of source neutron (n/sr/μC)	Detector position (distance from beam axis) (cm)					
				BC501A	Bonner[b]	F. C.[c]	TLD[d]	SSNTD[e]	Rem
43	0	0	3.15×10^{9}	-	-	0, 20	-	0	0
	0	80	3.45×10^{9}	20, 40	-	-	-	-	-
	10	0	3.15×10^{9}	0	-	0, 20	-	0	0
	10	70	3.45×10^{9}	20, 40	-	-	-	-	-
	20	0	3.15×10^{9}	0	0	0, 20	-	0	0
	20	60	3.45×10^{9}	20, 40	-	-	-	-	-
	40	0	3.15×10^{9}	0	0	0, 20	0	0	0
	40	40	3.45×10^{9}	20, 40	-	-	-	-	-
	70	0	3.15×10^{9}	0	-	0, 20	0	0	0
	100	0	3.15×10^{9}	0	0	-	0	0	0
67	0	0	4.00×10^{9}	-	-	0, 20	-	-	0
	0	80	4.77×10^{9}	20, 40	-	-	-	-	-
	20	0	4.00×10^{9}	0	0	0, 20	-	0	0
	20	60	4.77×10^{9}	20, 40	-	-	-	-	-
	40	0	4.00×10^{9}	0	0	0, 20	0	0	0
	40	40	4.77×10^{9}	20, 40	-	-	-	-	-
	70	0	4.00×10^{9}	0	-	0, 20	0	0	0
	100	0	4.00×10^{9}	0	0	0, 20	0	0	0
	130	0	4.00×10^{9}	0	-	20	0	0	0

[a] Proton energy.
[b] Bonner ball counter.
[c] ^{238}U and ^{232}Th fission counters.
[d] ^{7}LiF and ^{nat}LiF TLDs.
[e] Solid state nuclear track detector.
The BC501A, Bonner ball, fission and rem detectors were used for measurements behind the iron shields, and the TLD and SSNTD were used for measurements inside the iron shields of maximum thickness.

Table 2 Atomic compositions of the iron shield and the surrounding concrete.

Material	Atom	Atomic Density ($10^{22}cm^{-3}$)
Iron	Iron	8.487
Concrete	Hydrogen	1.498
	Oxygen	4.188
	Sodium	0.123
	Magnesium	0.062
	Aluminum	0.312
	Silicon	1.110
	Potassium	0.038
	Calcium	0.430
	Iron	0.141

Table 3 Source neutron energy spectrum via the $^{7}Li(p,n)$ reaction by 43-MeV protons.

Energy (MeV)	Flux (n/sr/MeV/μC)	Error	Energy (MeV)	Flux (n/sr/MeV/μC)	Error
5.00E+00*	5.69E-02	2.81E-03	2.60E+01	4.03E-02	1.83E-03
6.00E+00	4.72E-02	2.46E-03	2.70E+01	4.29E-02	2.18E-03
7.00E+00	4.60E-02	2.42E-03	2.80E+01	3.27E-02	1.53E-03
8.00E+00	4.38E-02	2.39E-03	2.90E+01	3.58E-02	1.72E-03
9.00E+00	4.41E-02	2.49E-03	3.00E+01	2.99E-02	1.70E-03
1.00E+01	4.54E-02	2.36E-03	3.10E+01	2.64E-02	1.74E-03
1.10E+01	4.48E-02	2.32E-03	3.20E+01	2.09E-02	1.12E-03
1.20E+01	4.37E-02	2.11E-03	3.30E+01	2.10E-02	1.54E-03
1.30E+01	4.68E-02	2.28E-03	3.40E+01	1.25E-02	1.17E-03
1.40E+01	4.71E-02	2.85E-03	3.50E+01	1.24E-02	1.15E-03
1.50E+01	5.34E-02	2.92E-03	3.60E+01	1.03E-02	7.33E-04
1.60E+01	5.31E-02	2.81E-03	3.70E+01	6.19E-03	7.80E-04
1.70E+01	4.63E-02	1.76E-03	3.80E+01	7.08E-03	8.18E-04
1.80E+01	5.19E-02	1.82E-03	3.90E+01	1.28E-01	3.41E-03
1.90E+01	4.94E-02	2.32E-03	4.00E+01	3.88E-01	5.81E-03
2.00E+01	4.82E-02	2.19E-03	4.10E+01	3.88E-01	4.73E-03
2.10E+01	4.83E-02	2.39E-03	4.20E+01	8.59E-02	2.65E-03
2.20E+01	4.70E-02	2.31E-03	4.30E+01	3.74E-03	5.46E-04
2.30E+01	4.76E-02	2.58E-03	4.40E+01	3.87E-04	1.73E-04
2.40E+01	4.53E-02	2.15E-03	4.50E+01	7.53E-05	7.53E-05
2.50E+01	4.20E-02	2.26E-03	4.60E+01	1.47E-04	1.04E-04

* Read as 5.00×10^{0}.

Table 4 Source neutron energy spectrum via the $^{7}Li(p,n)$ reaction by 68-MeV protons.

Energy (MeV)	Flux (n/sr/MeV/μC)	Error	Energy (MeV)	Flux (n/sr/MeV/μC)	Error
5.00E+00*	1.14E-02	1.74E-03	3.90E+01	3.36E-02	1.91E-03
6.00E+00	2.00E-02	1.59E-03	4.00E+01	3.48E-02	1.41E-03
7.00E+00	2.45E-02	1.53E-03	4.10E+01	3.45E-02	1.35E-03
8.00E+00	2.43E-02	1.55E-03	4.20E+01	3.44E-02	1.31E-03
9.00E+00	2.43E-02	1.55E-03	4.30E+01	3.01E-02	1.71E-03
1.00E+01	2.56E-02	1.59E-03	4.40E+01	3.29E-02	1.27E-03
1.10E+01	2.38E-02	1.52E-03	4.50E+01	3.06E-02	1.56E-03
1.20E+01	2.29E-02	1.51E-03	4.60E+01	3.14E-02	1.57E-03
1.30E+01	2.85E-02	1.73E-03	4.70E+01	3.05E-02	1.18E-03
1.40E+01	2.60E-02	1.63E-03	4.80E+01	3.07E-02	1.63E-03
1.50E+01	3.08E-02	1.78E-03	4.90E+01	2.97E-02	1.20E-03
1.60E+01	2.89E-02	1.71E-03	5.00E+01	2.71E-02	1.50E-03
1.70E+01	2.78E-02	1.69E-03	5.10E+01	2.97E-02	1.56E-03
1.80E+01	3.14E-02	1.84E-03	5.20E+01	2.56E-02	1.44E-03
1.90E+01	3.10E-02	1.91E-03	5.30E+01	2.67E-02	1.46E-03
2.00E+01	3.33E-02	1.97E-03	5.40E+01	2.30E-02	9.97E-04
2.10E+01	3.30E-02	1.98E-03	5.50E+01	2.14E-02	1.29E-03
2.20E+01	3.34E-02	1.93E-03	5.60E+01	2.05E-02	1.02E-03
2.30E+01	3.34E-02	1.77E-03	5.70E+01	1.61E-02	1.01E-03
2.40E+01	3.79E-02	2.01E-03	5.80E+01	1.22E-02	1.33E-03
2.50E+01	3.76E-02	1.94E-03	5.90E+01	1.46E-02	1.44E-03
2.60E+01	3.70E-02	1.95E-03	6.00E+01	7.50E-03	1.01E-03
2.70E+01	3.47E-02	1.89E-03	6.10E+01	9.05E-03	1.09E-03
2.80E+01	3.74E-02	1.92E-03	6.20E+01	7.72E-03	7.15E-04
2.90E+01	4.02E-02	2.09E-03	6.30E+01	3.40E-02	2.04E-03
3.00E+01	3.83E-02	1.74E-03	6.40E+01	2.28E-01	5.18E-03
3.10E+01	3.79E-02	1.77E-03	6.50E+01	3.61E-01	6.41E-03
3.20E+01	3.82E-02	1.79E-03	6.60E+01	2.59E-01	5.32E-03
3.30E+01	3.80E-02	1.75E-03	6.70E+01	7.43E-02	2.81E-03
3.40E+01	3.85E-02	1.93E-03	6.80E+01	9.98E-03	1.01E-03
3.50E+01	3.89E-02	2.21E-03	6.90E+01	1.25E-03	2.51E-04
3.60E+01	3.73E-02	1.75E-03	7.00E+01	6.29E-04	2.35E-04
3.70E+01	3.58E-02	1.88E-03	7.10E+01	1.87E-04	1.32E-04
3.80E+01	3.68E-02	1.78E-03	7.20E+01	9.09E-05	9.09E-05

* Read as 5.00×10^{0}.

Table 5 Calculated neutron response function of the Bonner ball counter.

Energy boundary (eV)	Neutron response (counts・cm^2)				
	Bare[a]	1.5cm[b]	3.0cm	5.0cm	9.0cm
4.00000E+08[c]	0.00000E+00	1.21200E-01	6.62394E-02	2.46543E-01	7.14114E-01
3.50000E+08	0.00000E+00	1.20400E-01	6.71040E-02	2.49249E-01	7.18918E-01
3.00000E+08	0.00000E+00	1.16800E-01	7.32570E-02	2.73726E-01	7.90511E-01
2.50000E+08	0.00000E+00	1.13100E-01	7.86617E-02	2.93372E-01	8.43989E-01
2.00000E+08	0.00000E+00	1.11000E-01	8.48387E-02	3.13194E-01	8.90955E-01
1.60000E+08	0.00000E+00	1.09000E-01	9.65422E-02	3.52922E-01	9.90692E-01
1.20000E+08	0.00000E+00	1.07200E-01	1.10366E-01	3.99808E-01	1.10748E+00
1.00000E+08	0.00000E+00	1.07200E-01	1.22603E-01	4.42516E-01	1.21633E+00
8.00000E+07	0.00000E+00	1.06900E-01	1.34893E-01	4.86849E-01	1.33248E+00
6.50000E+07	0.00000E+00	1.04900E-01	1.46848E-01	5.29604E-01	1.44291E+00
5.50000E+07	0.00000E+00	1.02400E-01	1.56024E-01	5.62324E-01	1.52658E+00
4.50000E+07	0.00000E+00	1.01800E-01	1.69035E-01	6.10579E-01	1.65795E+00
3.50000E+07	3.08890E-03	1.18500E-01	1.99471E-01	7.19847E-01	1.94066E+00
2.75000E+07	7.92810E-03	1.15400E-01	2.40935E-01	8.64964E-01	2.29764E+00
2.25000E+07	1.13260E-02	1.28400E-01	3.16469E-01	1.11515E+00	2.85595E+00
1.75000E+07	1.72980E-02	1.39600E-01	4.24644E-01	1.43829E+00	3.48625E+00
1.35000E+07	2.31320E-02	1.26300E-01	5.34824E-01	1.75848E+00	4.09864E+00
1.00000E+07	3.07170E-02	1.54100E-01	7.92599E-01	2.49755E+00	5.32674E+00
6.70000E+06	3.90230E-02	2.39900E-01	1.27319E+00	3.72114E+00	6.94474E+00
4.49000E+06	4.69170E-02	3.50900E-01	1.83004E+00	4.88226E+00	7.67178E+00
3.01000E+06	5.28540E-02	5.12600E-01	2.58673E+00	6.31731E+00	8.51392E+00
2.02000E+06	5.47420E-02	7.28600E-01	3.48174E+00	7.72055E+00	8.76757E+00
1.35000E+06	3.31540E-02	9.76200E-01	4.42043E+00	8.78493E+00	8.18403E+00
9.07000E+05	1.55820E-02	1.38700E+00	5.53914E+00	9.55978E+00	6.95255E+00
4.98000E+05	1.83100E-02	2.08400E+00	6.80840E+00	9.76846E+00	5.16499E+00
2.24000E+05	2.81430E-02	2.92200E+00	7.76509E+00	9.24283E+00	3.61335E+00
8.65000E+04	6.64210E-02	3.94900E+00	8.48133E+00	8.39302E+00	2.57384E+00
1.50000E+04	1.61590E-01	5.17500E+00	9.25074E+00	7.86099E+00	2.04393E+00
3.35000E+03	4.01050E-01	6.59600E+00	1.00090E+01	7.47934E+00	1.74043E+00
4.54000E+02	1.57150E+00	8.54800E+00	1.06606E+01	6.70883E+00	1.38113E+00
2.26000E+01	4.53720E+00	1.17100E+01	1.03980E+01	5.53631E+00	1.03592E+00
5.04000E+00	9.59580E+00	1.23900E+01	9.08346E+00	4.43734E+00	8.04266E-01
1.12000E+00	1.75920E+01	7.94100E+00	6.99154E+00	3.25360E+00	5.81233E-01
4.14000E-01					

[a] Response function of He^3 conuter (10atm).

[b] Thickness of moderator of the Bonner ball counter.

[c] Read as 4.0000×10^8.

Table 6 Fission cross sections of ^{232}Th and ^{238}U.

Energy boundary (eV)	Cross section (b) ^{232}Th	^{238}U	Energy boundary (eV)	Cross section (b) ^{232}Th	^{238}U
4.00000E+08*	5.79150E-01	1.30160E+00	1.22000E+07	3.12670E-01	9.78590E-01
3.75000E+08	6.63800E-01	1.31280E+00	1.00000E+07	3.36980E-01	9.90390E-01
3.50000E+08	7.40800E-01	1.32960E+00	8.19000E+06	3.87460E-01	9.75730E-01
3.25000E+08	7.68010E-01	1.33940E+00	6.70000E+06	1.99310E-01	6.56390E-01
3.00000E+08	7.83760E-01	1.34340E+00	5.49000E+06	1.49680E-01	5.37130E-01
2.75000E+08	8.00470E-01	1.33340E+00	4.49000E+06	1.46240E-01	5.61180E-01
2.50000E+08	8.09150E-01	1.32540E+00	3.68000E+06	1.45990E-01	5.33830E-01
2.25000E+08	8.17960E-01	1.32240E+00	3.01000E+06	1.27970E-01	5.38620E-01
2.00000E+08	7.34890E-01	1.32440E+00	2.46000E+06	1.27120E-01	5.49190E-01
1.80000E+08	7.74710E-01	1.31940E+00	2.02000E+06	1.03150E-01	4.95590E-01
1.60000E+08	7.53110E-01	1.32270E+00	1.65000E+06	8.38190E-02	3.14610E-01
1.40000E+08	8.04100E-01	1.35160E+00	1.35000E+06	1.35510E-02	5.16710E-02
1.20000E+08	7.83140E-01	1.35830E+00	1.11000E+06	1.78060E-03	1.89980E-02
1.10000E+08	8.08390E-01	1.41800E+00	9.07000E+05	5.96400E-04	6.52920E-03
1.00000E+08	8.42850E-01	1.44930E+00	7.43000E+05	1.19900E-04	1.03340E-03
9.00000E+07	8.65330E-01	1.48450E+00	4.98000E+05	1.29510E-05	2.57700E-04
8.00000E+07	8.73280E-01	1.52340E+00	3.34000E+05	0.00000E+00	9.61590E-05
7.00000E+07	8.98510E-01	1.53830E+00	2.24000E+05	0.00000E+00	9.90000E-05
6.50000E+07	9.04060E-01	1.58930E+00	1.50000E+05	0.00000E+00	3.95290E-05
6.00000E+07	8.72160E-01	1.63950E+00	8.65000E+04	0.00000E+00	6.12950E-05
5.50000E+07	7.91730E-01	1.64420E+00	3.18000E+04	0.00000E+00	9.63850E-05
5.00000E+07	8.29780E-01	1.66560E+00	1.50000E+04	0.00000E+00	1.10100E-04
4.50000E+07	8.34770E-01	1.68560E+00	7.10000E+03	0.00000E+00	6.72000E-06
4.00000E+07	7.84670E-01	1.67380E+00	3.35000E+03	0.00000E+00	4.00000E-08
3.50000E+07	7.56860E-01	1.66210E+00	1.58000E+03	0.00000E+00	4.56240E-08
3.00000E+07	6.54610E-01	1.61730E+00	4.54000E+02	0.00000E+00	8.71180E-08
2.75000E+07	6.46350E-01	1.58130E+00	1.01000E+02	0.00000E+00	1.81650E-07
2.50000E+07	6.48010E-01	1.57170E+00	2.26000E+01	0.00000E+00	3.09570E-07
2.25000E+07	5.80630E-01	1.47480E+00	1.07000E+01	0.00000E+00	4.47160E-07
1.96000E+07	5.08630E-01	1.21330E+00	5.04000E+00	0.00000E+00	6.46250E-07
1.75000E+07	4.42260E-01	1.23440E+00	2.38000E+00	0.00000E+00	9.34230E-07
1.49000E+07	3.71200E-01	1.13580E+00	1.12000E+00	0.00000E+00	1.43970E-06
1.35000E+07	3.19230E-01	1.00340E+00	4.14000E-01	0.00000E+00	6.36560E-06

* Read as 4.00000 x 10^8.

Lower energy boundary is 1.00000E-04 (eV).

Table 7 Calculated neutron responses of ^{7}LiF and ^{nat}LiF TLDs.

Energy (MeV)	Response (^{60}Coeq. R・cm^2) ^{7}LiF	^{nat}LiF	Energy (MeV)	Response (^{60}Coeq. R・cm^2) ^{7}LiF	^{nat}LiF	Energy (MeV)	Response (^{60}Coeq. R・cm^2) ^{7}LiF	^{nat}LiF
1.649E+01*	6.450E-10	6.800E-10	9.804E-02	1.077E-11	4.642E-11	2.902E-05	1.722E-12	1.287E-09
1.455E+01	5.662E-10	5.988E-10	8.652E-02	9.631E-12	4.419E-11	2.260E-05	1.949E-12	1.459E-09
1.284E+01	5.662E-10	5.988E-10	7.635E-02	5.039E-12	3.933E-11	1.760E-05	2.208E-12	1.653E-09
1.133E+01	5.204E-10	5.533E-10	6.738E-02	3.437E-12	3.802E-11	1.371E-05	2.501E-12	1.874E-09
1.000E+01	4.688E-10	5.028E-10	5.946E-02	2.820E-12	3.813E-11	1.068E-05	2.834E-12	2.124E-09
8.825E+00	4.099E-10	4.437E-10	5.946E-02	2.806E-12	3.917E-11	8.315E-06	3.211E-12	2.407E-09
7.788E+00	3.442E-10	3.767E-10	5.248E-02	2.806E-12	3.917E-11	6.476E-06	3.638E-12	2.727E-09
6.873E+00	2.990E-10	3.290E-10	4.631E-02	5.361E-12	4.302E-11	5.044E-06	4.122E-12	3.090E-09
6.065E+00	2.530E-10	2.804E-10	4.087E-02	2.579E-12	4.182E-11	3.928E-06	4.671E-12	3.502E-09
5.353E+00	2.186E-10	2.438E-10	3.607E-02	2.136E-12	4.319E-11	3.059E-06	5.292E-12	3.968E-09
4.724E+00	1.719E-10	1.949E-10	3.183E-02	1.709E-12	4.478E-11	2.382E-06	5.997E-12	4.497E-09
4.169E+00	1.543E-10	1.751E-10	2.809E-02	1.787E-12	4.710E-11	1.855E-06	6.798E-12	5.097E-09
3.679E+00	1.311E-10	1.500E-10	2.479E-02	3.036E-12	5.080E-11	1.445E-06	7.700E-12	5.774E-09
3.247E+00	1.218E-10	1.387E-10	2.187E-02	1.440E-12	5.188E-11	1.125E-06	8.728E-12	6.545E-09
2.865E+00	1.167E-10	1.315E-10	1.931E-02	1.141E-12	5.447E-11	8.764E-07	9.887E-12	7.414E-09
2.528E+00	1.152E-10	1.296E-10	1.704E-02	1.008E-12	5.742E-11	6.826E-07	1.120E-11	8.402E-09
2.231E+00	1.036E-10	1.194E-10	1.503E-02	9.274E-13	6.068E-11	5.316E-07	1.270E-11	9.523E-09
1.969E+00	9.057E-11	1.079E-10	1.171E-02	8.537E-13	6.615E-11	4.140E-07	1.438E-11	1.078E-08
1.738E+00	7.836E-11	9.669E-11	9.119E-03	6.922E-13	7.420E-11	1.518E-07	1.987E-11	1.490E-08
1.533E+00	7.452E-11	9.239E-11	7.102E-03	5.449E-13	8.350E-11	3.524E-10	3.417E-11	2.562E-08
1.353E+00	6.543E-11	8.192E-11	5.531E-03	4.637E-13	9.415E-11			
1.194E+00	6.315E-11	7.871E-11	4.307E-03	4.080E-13	1.063E-10			
1.054E+00	5.453E-11	6.968E-11	3.355E-03	3.705E-13	1.202E-10			
9.301E-01	4.677E-11	6.197E-11	2.613E-03	3.480E-13	1.360E-10			
8.209E-01	4.075E-11	5.634E-11	2.035E-03	3.377E-13	1.539E-10			
7.244E-01	3.592E-11	5.216E-11	1.585E-03	3.379E-13	1.743E-10			
6.393E-01	2.844E-11	4.562E-11	1.234E-03	3.476E-13	1.974E-10			
5.642E-01	2.782E-11	4.650E-11	9.611E-04	3.661E-13	2.236E-10			
4.979E-01	2.699E-11	4.797E-11	7.485E-04	3.927E-13	2.533E-10			
4.394E-01	2.504E-11	4.957E-11	5.830E-04	4.274E-13	2.871E-10			
3.877E-01	2.682E-11	5.750E-11	4.540E-04	4.710E-13	3.253E-10			
3.422E-01	2.670E-11	6.879E-11	3.536E-04	5.227E-13	3.686E-10			
3.020E-01	2.804E-11	9.309E-11	2.754E-04	5.831E-13	4.177E-10			
2.665E-01	3.821E-11	1.504E-10	2.145E-04	6.532E-13	4.734E-10			
2.352E-01	3.585E-11	2.090E-10	1.670E-04	7.336E-13	5.365E-10			
2.075E-01	1.700E-11	1.769E-10	1.301E-04	8.262E-13	6.081E-10			
1.832E-01	1.121E-11	1.142E-10	1.013E-04	9.317E-13	6.891E-10			
1.616E-01	9.773E-12	7.795E-11	7.889E-05	1.052E-12	7.810E-10			
1.426E-01	8.753E-12	5.982E-11	6.144E-05	1.188E-12	8.847E-10			
1.259E-01	6.867E-12	4.940E-11	4.785E-05	1.344E-12	1.002E-09			
1.111E-01	6.706E-12	4.474E-11	3.727E-05	1.521E-12	1.136E-09			

* Read as 1.649×10^{1}.

Table 8 Calculated neutron response of solid state nuclear track detector (TS-16N).

Energy (MeV)	Response (Pits/n)	Energy (MeV)	Response (Pits/n)
1.00E-01	3.643E-04	3.44E+00	9.508E-04
2.00E-01	4.915E-04	3.52E+00	9.239E-04
3.50E-01	5.325E-04	3.80E+00	9.156E-04
4.35E-01	6.589E-04	4.00E-00	9.446E-04
5.00E-01	5.010E-04	4.27E+00	9.517E-04
6.00E-01	5.339E-04	5.00E+00	9.364E-04
8.00E-01	5.521E-04	6.00E+00	9.546E-04
1.00E+00	6.271E-04	6.295E+0	1.017E-03
1.22E+00	6.015E-04	7.00E+00	9.429E-04
1.32E+00	6.948E-04	7.745E+0	9.841E-04
1.65E+00	7.587E-04	8.00E+00	9.439E-04
2.00E+00	7.069E-04	1.00E+01	8.858E-04
2.077E+0	8.293E-04	1.20E+01	7.327E-04
2.35E+00	7.368E-04	1.50E+01	2.845E-04
2.815E+0	8.928E-04	1.60E+01	2.411E-04
2.944E+0	8.664E-04	1.875E+1	2.210E-04
3.00E+00	7.964E-04	2.00E+01	2.161E-04
3.21E+00	8.769E-04		

* Read as 1.00×10^{-1}.

Table 9 Measured neutron spectra behind 0cm thick iron by the BC501A detector for 43-MeV p-Li neutrons.

Energy (eV)	Neutron Flux (n/cm^2/Lethargy/μC)	Error (%)	Neutron Flux (n/cm^2/Lethargy/μC)	Error (%)
	20 cm from beam axis		40 cm from beam axis	
4.8E+7*	1.112E+0	4.162E-1	1.467E-1	2.505E-1
4.6E+7	1.957E+0	4.454E-1	2.764E-1	2.231E-1
4.4E+7	5.473E+0	3.124E-1	6.266E-1	1.696E-1
4.3E+7	1.761E+1	1.133E-1	1.245E+0	1.433E-1
4.2E+7	4.183E+1	8.159E-2	2.114E+0	1.177E-1
4.1E+7	6.240E+1	8.521E-2	3.168E+0	1.149E-1
4.0E+7	6.127E+1	6.179E-2	4.118E+0	8.230E-2
3.9E+7	4.950E+1	9.929E-2	3.993E+0	8.522E-2
3.8E+7	3.995E+1	1.767E-1	2.635E+0	2.395E-1
3.7E+7	2.677E+1	2.469E-1	1.360E+0	3.963E-1
3.6E+7	1.396E+1	1.300E-1	9.061E-1	1.413E-1
3.5E+7	9.106E+0	2.147E-1	9.192E-1	1.891E-1
3.4E+7	9.402E+0	2.237E-1	1.016E+0	1.798E-1
3.3E+7	1.070E+1	1.706E-1	1.086E+0	1.466E-1
3.2E+7	1.176E+1	1.431E-1	1.123E+0	1.323E-1
3.1E+7	1.252E+1	1.154E-1	1.140E+0	1.125E-1
3.0E+7	1.307E+1	7.447E-2	1.150E+0	7.536E-2
2.9E+7	1.343E+1	4.320E-2	1.172E+0	4.491E-2
2.8E+7	1.354E+1	4.793E-2	1.217E+0	4.811E-2
2.7E+7	1.341E+1	9.657E-2	1.289E+0	8.922E-2
2.6E+7	1.316E+1	1.653E-1	1.367E+0	1.413E-1
2.5E+7	1.297E+1	2.033E-1	1.426E+0	1.649E-1
2.4E+7	1.290E+1	1.888E-1	1.455E+0	1.496E-1
2.3E+7	1.280E+1	1.396E-1	1.458E+0	1.097E-1
2.2E+7	1.258E+1	8.037E-2	1.447E+0	6.308E-2
2.1E+7	1.227E+1	2.396E-2	1.420E+0	2.042E-2
2.0E+7	1.203E+1	6.328E-2	1.378E+0	4.999E-2
1.9E+7	1.194E+1	1.268E-1	1.335E+0	1.006E-1
1.8E+7	1.178E+1	1.413E-1	1.311E+0	1.121E-1
1.7E+7	1.131E+1	8.077E-2	1.306E+0	6.126E-2
1.6E+7	1.060E+1	3.715E-2	1.301E+0	2.797E-2
1.5E+7	1.009E+1	7.698E-2	1.284E+0	5.445E-2
1.4E+7	1.004E+1	2.572E-2	1.265E+0	1.907E-2
1.3E+7	1.031E+1	5.685E-2	1.265E+0	4.170E-2
1.2E+7	1.052E+1	8.643E-2	1.285E+0	6.318E-2
1.1E+7	1.049E+1	7.407E-2	1.309E+0	5.319E-2
1.0E+7	1.049E+1	4.992E-2	1.339E+0	3.532E-2
9.0E+6	1.086E+1	3.583E-2	1.416E+0	2.484E-2
8.0E+6	1.134E+1	1.429E-2	1.560E+0	9.917E-3
7.0E+6	1.072E+1	1.709E-1	1.617E+0	1.009E-1
6.0E+6	7.637E+0	3.903E-1	1.258E+0	2.107E-1
5.0E+6				

* Read as 4.8×10^7.

Table 10 Measured neutron spectra behind 10cm thick iron by the BC501A detector for 43-MeV p-Li neutrons.

Energy (eV)	Neutron Flux (n/cm^2/Lethargy/μC)	Error (%)	Neutron Flux (n/cm^2/Lethargy/μC)	Error (%)	Neutron Flux (n/cm^2/Lethargy/μC)	Error (%)
	beam axis		20 cm from beam axis		40 cm from beam axis	
4.4E+7*	4.695E+3	1.105E-1	2.396E+1	3.087E-1	2.635E+0	2.287E-1
4.3E+7	1.252E+4	6.413E-2	7.559E+1	1.012E-1	6.868E+0	1.203E-1
4.2E+7	2.758E+4	2.633E-2	1.920E+2	7.276E-2	1.373E+1	9.192E-2
4.1E+7	4.193E+4	2.473E-2	2.931E+2	7.516E-2	1.856E+1	1.026E-1
4.0E+7	4.114E+4	3.729E-2	2.657E+2	5.145E-2	1.809E+1	8.364E-2
3.9E+7	2.513E+4	4.115E-2	1.903E+2	1.068E-1	1.515E+1	1.154E-1
3.8E+7	9.753E+3	2.811E-2	1.714E+2	1.461E-1	1.172E+1	2.341E-1
3.7E+7	3.267E+3	1.159E-1	1.388E+2	1.818E-1	7.727E+0	3.222E-1
3.6E+7	2.097E+3	1.667E-1	7.978E+1	9.382E-2	4.999E+0	1.306E-1
3.5E+7	2.275E+3	1.057E-1	5.030E+1	1.381E-1	4.456E+0	1.693E-1
3.4E+7	2.613E+3	7.191E-2	4.817E+1	1.592E-1	5.002E+0	1.616E-1
3.3E+7	2.951E+3	8.780E-2	5.272E-1	1.274E-1	5.704E+0	1.237E-1
3.2E+7	3.261E+3	1.075E-1	5.719E-1	1.086E-1	6.258E-0	1.049E-1
3.1E+7	3.504E+3	1.005E-1	6.105E+1	8.719E-2	6.583E+0	8.584E-2
3.0E+7	3.661E+3	6.812E-2	6.430E+1	5.558E-2	6.706E+0	5.686E-2
2.9E+7	3.779E+3	3.930E-2	6.659E+1	3.182E-2	6.770E+0	3.388E-2
2.8E+7	3.945E+3	4.375E-2	6.755E+1	3.509E-2	6.952E+0	3.675E-2
2.7E+7	4.190E+3	8.587E-2	6.730E+1	7.158E-2	7.304E+0	6.951E-2
2.6E+7	4.418E+3	1.379E-1	6.648E+1	1.219E-1	7.686E+0	1.110E-1
2.5E+7	4.476E+3	1.651E-1	6.569E+1	1.496E-1	7.899E+0	1.313E-1
2.4E+7	4.303E+3	1.589E-1	6.494E+1	1.397E-1	7.862E+0	1.218E-1
2.3E+7	3.988E+3	1.254E-1	6.395E+1	1.041E-1	7.630E+0	9.225E-2
2.2E+7	3.660E+3	7.648E-2	6.274E+1	6.025E-2	7.285E+0	5.476E-2
2.1E+7	3.368E+3	2.067E-2	6.171E+1	1.770E-2	6.854E+0	1.779E-2
2.0E+7	3.087E+3	7.123E-2	6.117E+1	4.612E-2	6.346E+0	4.743E-2
1.9E+7	2.816E+3	1.532E-1	6.081E+1	9.268E-2	5.867E+0	1.013E-1
1.8E+7	2.616E+3	1.789E-1	5.974E+1	1.039E-1	5.625E+0	1.160E-1
1.7E+7	2.524E+3	9.818E-2	5.734E+1	5.968E-2	5.712E+0	6.255E-2
1.6E+7	2.456E+3	4.116E-2	5.422E+1	2.689E-2	5.895E+0	2.675E-2
1.5E+7	2.281E+3	9.553E-2	5.221E+1	5.516E-2	5.828E+0	5.273E-2
1.4E+7	1.993E+3	3.369E-2	5.256E+1	1.837E-2	5.494E+0	1.911E-2
1.3E+7	1.725E+3	9.565E-2	5.420E+1	4.011E-2	5.223E+0	4.444E-2
1.2E+7	1.537E+3	1.665E-1	5.469E+1	6.175E-2	5.222E+0	6.865E-2
1.1E+7	1.346E+3	1.617E-1	5.355E+1	5.391E-2	5.405E+0	5.678E-2
1.0E+7	1.118E+3	1.301E-1	5.277E+1	3.686E-2	5.652E+0	3.675E-2
9.0E+6	9.082E+2	1.146E-1	5.392E+1	2.680E-2	5.974E+0	2.585E-2
8.0E+6	7.898E+2	6.252E-2	5.626E+1	1.066E-2	6.629E+0	1.003E-2
7.0E+6	7.640E+2	4.541E-1	5.406E+1	1.260E-1	7.374E+0	9.782E-2
6.0E+6	5.555E+2	1.565E-1	3.922E+1	2.825E-1	6.299E+0	1.862E-1
5.0E+6						

* Read as 4.4×10^7.

Table 11 Measured neutron spectra behind 20cm thick iron by the BC501A detector for 43-MeV p-Li neutrons.

Energy (eV)	Neutron Flux (n/cm^2/Lethargy/μC)	Error (%)	Neutron Flux (n/cm^2/Lethargy/μC)	Error (%)	Neutron Flux (n/cm^2/Lethargy/μC)	Error (%)
	beam axis		20 cm from beam axis		40 cm from beam axis	
4.4E+7*	1.115E+3	1.658E-1	2.763E+1	8.426E-2	2.366E+0	2.393E-1
4.3E+7	3.220E+3	2.303E-1	7.307E+1	5.719E-2	5.772E+0	2.517E-1
4.2E+7	7.499E+3	1.842E-1	1.519E+2	3.915E-2	1.170E+1	2.913E-1
4.1E+7	1.127E+4	9.973E-2	2.250E+2	3.977E-2	1.650E+1	1.589E-1
4.0E+7	1.007E+4	5.362E-2	2.416E+2	3.737E-2	1.689E+1	1.349E-1
3.9E+7	5.012E+3	3.320E-1	2.052E+2	4.084E-2	1.366E+1	2.029E-1
3.8E+7	1.430E+3	8.762E-1	1.487E+2	1.171E-1	8.946E+0	3.234E-1
3.7E+7	6.438E+2	3.978E-1	9.034E+1	1.604E-1	5.399E+0	5.833E-1
3.6E+7	7.633E+2	3.453E-1	5.127E+1	6.232E-2	4.161E+0	1.973E-1
3.5E+7	8.491E+2	3.601E-1	3.940E+1	1.215E-1	4.108E+0	2.060E-1
3.4E+7	8.753E+2	2.645E-1	4.079E+1	1.243E-1	4.204E+0	2.202E-1
3.3E+7	8.917E+2	1.769E-1	4.410E+1	1.027E-1	4.195E+0	1.815E-1
3.2E+7	9.053E+2	1.240E-1	4.627E+1	9.334E-2	4.135E+0	1.599E-1
3.1E+7	9.148E+2	9.808E-2	4.713E+1	7.984E-2	4.116E+0	1.337E-1
3.0E+7	9.240E+2	8.781E-2	4.707E+1	5.360E-2	4.173E+0	8.847E-2
2.9E+7	9.416E+2	9.660E-2	4.662E+1	3.205E-2	4.246E+0	5.539E-2
2.8E+7	9.734E+2	1.255E-1	4.630E+1	3.603E-2	4.236E+0	6.615E-2
2.7E+7	1.014E+3	1.647E-1	4.636E+1	7.289E-2	4.122E+0	1.275E-1
2.6E+7	1.044E+3	1.986E-1	4.661E+1	1.223E-1	4.001E+0	2.126E-1
2.5E+7	1.046E+3	2.151E-1	4.642E+1	1.491E-1	3.974E+0	2.562E-1
2.4E+7	1.011E+3	2.077E-1	4.527E+1	1.409E-1	4.034E+0	2.321E-1
2.3E+7	9.449E+2	1.740E-1	4.316E+1	1.085E-1	4.093E+0	1.687E-1
2.2E+7	8.609E+2	1.104E-1	4.064E+1	6.538E-2	4.103E+0	9.766E-2
2.1E+7	7.706E+2	2.723E-2	3.828E+1	1.918E-2	4.106E+0	3.137E-2
2.0E+7	6.860E+2	1.025E-1	3.625E+1	5.537E-2	4.170E+0	6.969E-2
1.9E+7	6.189E+2	1.916E-1	3.446E+1	1.149E-1	4.264E+0	1.389E-1
1.8E+7	5.765E+2	2.005E-1	3.298E+1	1.310E-1	4.231E+0	1.570E-1
1.7E+7	5.505E+2	1.198E-1	3.192E+1	7.268E-2	3.941E+0	9.645E-2
1.6E+7	5.192E+2	3.438E-2	3.112E+1	3.150E-2	3.507E+0	4.175E-2
1.5E+7	4.663E+2	4.778E-2	3.040E+1	6.701E-2	3.222E+0	9.230E-2
1.4E+7	3.969E+2	2.643E-2	2.987E+1	2.169E-2	3.235E+0	3.323E-2
1.3E+7	3.283E+2	1.493E-1	2.964E+1	5.175E-2	3.406E+0	6.509E-2
1.2E+7	2.701E+2	2.712E-1	2.932E+1	8.128E-2	3.495E+0	9.960E-2
1.1E+7	2.213E+2	3.230E-1	2.847E+1	7.158E-2	3.423E+0	8.615E-2
1.0E+7	1.797E+2	3.148E-1	2.753E+1	4.987E-2	3.324E+0	5.927E-2
9.0E+6	1.520E+2	1.786E-1	2.750E+1	3.698E-2	3.378E+0	4.384E-2
8.0E+6	1.508E+2	2.753E-1	2.871E+1	1.441E-2	3.451E+0	1.769E-2
7.0E+6	1.496E+2	5.629E-1	2.900E+1	1.657E-1	2.960E+0	2.362E-1
6.0E+6	9.150E+1	2.326E-1	2.271E+1	3.437E-1	1.755E+0	6.519E-1
5.0E+6						

* Read as 4.4×10^7.

Table 12 Measured neutron spectra behind 40cm thick iron by the BC501A detector for 43-MeV p-Li neutrons.

Energy (eV)	Neutron Flux (n/cm^2/Lethargy/μC)	Error (%)	Neutron Flux (n/cm^2/Lethargy/μC)	Error (%)	Neutron Flux (n/cm^2/Lethargy/μC)	Error (%)
	beam axis		20 cm from beam axis		40 cm from beam axis	
4.4E+7*	6.705E+1	1.254E-1	6.384E+0	1.584E-1	9.880E-1	2.113E-1
4.3E+7	1.942E+2	5.757E-2	1.805E+1	1.003E-1	2.025E+0	1.215E-1
4.2E+7	3.922E+2	2.583E-2	3.981E+1	6.571E-2	3.880E+0	1.063E-1
4.1E+7	5.260E+2	3.384E-2	6.085E+1	6.403E-2	5.927E+0	1.076E-1
4.0E+7	4.591E+2	5.254E-2	6.408E+1	6.005E-2	6.529E+0	6.686E-2
3.9E+7	2.541E+2	6.305E-2	4.998E+1	7.361E-2	4.882E+0	1.205E-1
3.8E+7	8.991E+1	4.738E-2	3.292E+1	2.248E-1	2.641E+0	2.996E-1
3.7E+7	2.836E+1	1.806E-1	1.996E+1	3.088E-1	1.568E+0	4.851E-1
3.6E+7	2.073E+1	2.514E-1	1.254E+1	1.109E-1	1.467E+0	1.479E-1
3.5E+7	2.562E+1	1.586E-1	1.017E+1	2.006E-1	1.549E+0	1.407E-1
3.4E+7	3.105E+1	1.048E-1	1.013E+1	2.092E-1	1.559E+0	1.506E-1
3.3E+7	3.532E+1	8.737E-2	1.052E+1	1.732E-1	1.512E+0	1.329E-1
3.2E+7	3.842E+1	8.178E-2	1.082E+1	1.558E-1	1.440E+0	1.269E-1
3.1E+7	4.055E+1	7.499E-2	1.093E+1	1.328E-1	1.361E+0	1.145E-1
3.0E+7	4.183E+1	6.859E-2	1.085E+1	9.031E-2	1.294E+0	8.122E-2
2.9E+7	4.234E+1	7.211E-2	1.064E+1	5.566E-2	1.243E+0	5.101E-2
2.8E+7	4.217E+1	9.123E-2	1.039E+1	6.295E-2	1.206E+0	5.848E-2
2.7E+7	4.157E+1	1.240E-1	1.015E+1	1.266E-1	1.174E+0	1.186E-1
2.6E+7	4.080E+1	1.569E-1	9.899E+0	2.185E-1	1.145E+0	2.043E-1
2.5E+7	4.001E+1	1.743E-1	9.555E+0	2.752E-1	1.118E+0	2.540E-1
2.4E+7	3.912E+1	1.662E-1	9.052E+0	2.684E-1	1.093E+0	2.400E-1
2.3E+7	3.807E+1	1.329E-1	8.405E+0	2.120E-1	1.063E+0	1.813E-1
2.2E+7	3.685E+1	7.872E-2	7.717E+0	1.302E-1	1.019E+0	1.076E-1
2.1E+7	3.559E+1	1.773E-2	7.102E+0	4.051E-2	9.532E-1	3.452E-2
2.0E+7	3.418E+1	6.328E-2	6.583E+0	1.160E-1	8.708E-1	9.456E-2
1.9E+7	3.227E+1	1.111E-1	6.141E+0	2.451E-1	7.861E-1	2.072E-1
1.8E+7	2.941E+1	1.166E-1	5.820E+0	2.830E-1	7.220E-1	2.481E-1
1.7E+7	2.568E+1	7.266E-2	5.646E+0	1.577E-1	6.938E-1	1.423E-1
1.6E+7	2.183E+1	2.187E-2	5.491E+0	7.144E-2	6.917E-1	6.311E-2
1.5E+7	1.882E+1	3.802E-2	5.228E+0	1.489E-1	6.907E-1	1.211E-1
1.4E+7	1.699E+1	1.928E-2	4.944E+0	5.069E-2	6.809E-1	4.061E-2
1.3E+7	1.587E+1	9.710E-2	4.742E+0	1.235E-1	6.726E-1	9.368E-2
1.2E+7	1.465E+1	1.569E-1	4.485E+0	2.023E-1	6.706E-1	1.457E-1
1.1E+7	1.284E+1	1.753E-1	4.084E+0	1.900E-1	6.622E-1	1.262E-1
1.0E+7	1.069E+1	1.668E-1	3.817E+0	1.371E-1	6.439E-1	8.748E-2
9.0E+6	8.595E+0	9.798E-2	3.884E+0	9.972E-2	6.454E-1	6.466E-2
8.0E+6	6.529E+0	2.016E-1	4.218E+0	3.760E-2	6.952E-1	2.487E-2
7.0E+6	5.532E+0	5.356E-1	4.562E+0	4.007E-1	7.319E-1	2.690E-1
6.0E+6	6.227E+0	3.653E-1	3.857E+0	7.700E-1	5.873E-1	5.452E-1
5.0E+6						

* Read as 4.4×10^7.

Table 13 Measured neutron spectrum behind 70cm thick iron by the BC501A detector for 43-MeV p-Li neutrons.

Energy (eV)	Neutron Flux (n/cm^2/Lethargy/μC)	Error (%)
	beam axis	
4.6E+7*	8.704E-2	9.535E-1
4.4E+7	3.359E-1	2.059E-1
4.3E+7	1.162E+0	1.431E-1
4.2E+7	2.788E+0	1.217E-1
4.1E+7	4.376E+0	7.911E-2
4.0E+7	5.009E+0	6.963E-2
3.9E+7	4.954E+0	7.107E-2
3.8E+7	4.194E+0	1.503E-1
3.7E+7	2.526E+0	2.110E-1
3.6E+7	1.052E+0	1.135E-1
3.5E+7	5.042E-1	3.516E-1
3.4E+7	4.668E-1	3.903E-1
3.3E+7	5.141E-1	2.996E-1
3.2E+7	5.474E-1	2.576E-1
3.1E+7	5.823E-1	2.085E-1
3.0E+7	6.305E-1	1.300E-1
2.9E+7	6.684E-1	7.564E-2
2.8E+7	6.571E-1	8.621E-2
2.7E+7	5.881E-1	1.848E-1
2.6E+7	4.998E-1	3.637E-1
2.5E+7	4.403E-1	5.008E-1
2.4E+7	4.234E-1	4.811E-1
2.3E+7	4.320E-1	3.456E-1
2.2E+7	4.520E-1	1.866E-1
2.1E+7	4.869E-1	5.132E-2
2.0E+7	5.436E-1	1.179E-1
1.9E+7	6.000E-1	2.100E-1
1.8E+7	5.947E-1	2.319E-1
1.7E+7	4.845E-1	1.546E-1
1.6E+7	3.261E-1	1.014E-1
1.5E+7	2.441E-1	2.678E-1
1.4E+7	2.837E-1	7.452E-2
1.3E+7	3.569E-1	1.371E-1
1.2E+7	3.697E-1	2.053E-1
1.1E+7	3.227E-1	2.013E-1
1.0E+7	2.761E-1	1.589E-1
9.0E+6	2.695E-1	1.205E-1
8.0E+6	2.355E-1	5.618E-2
7.0E+6	6.468E-2	2.365E+0
6.0E+6		

* Read as 4.6×10^7.

Table 14 Measured neutron spectrum behind 100cm thick iron by the BC501A detector for 43-MeV p-Li neutrons.

Energy (eV)	Neutron Flux (n/cm^2/Lethargy/μC)	Error (%)
	beam axis	
4.4E+7*	2.330E-2	8.953E-1
4.3E+7	4.232E-2	8.537E-1
4.2E+7	6.126E-2	5.806E-1
4.1E+7	7.291E-2	2.275E-1
4.0E+7	7.272E-2	1.965E-1
3.9E+7	6.116E-2	4.612E-1
3.8E+7	4.342E-2	6.023E-1
3.7E+7	2.672E-2	5.509E-1
3.6E+7	1.597E-2	3.607E-1
3.5E+7	1.158E-2	4.789E-1
3.4E+7	1.104E-2	5.065E-1
3.3E+7	1.185E-2	3.723E-1
3.2E+7	1.270E-2	2.487E-1
3.1E+7	1.315E-2	1.771E-1
3.0E+7	1.311E-2	1.487E-1
2.9E+7	1.257E-2	1.495E-1
2.8E+7	1.161E-2	1.702E-1
2.7E+7	1.043E-2	2.119E-1
2.6E+7	9.328E-3	2.691E-1
2.5E+7	8.538E-3	3.117E-1
2.4E+7	8.081E-3	3.074E-1
2.3E+7	7.767E-3	2.565E-1
2.2E+7	7.372E-3	1.865E-1
2.1E+7	6.840E-3	1.439E-1
2.0E+7	6.300E-3	2.179E-1
1.9E+7	5.889E-3	2.943E-1
1.8E+7	5.617E-3	2.996E-1
1.7E+7	5.432E-3	2.378E-1
1.6E+7	5.353E-3	1.664E-1
1.5E+7	5.409E-3	1.325E-1
1.4E+7	5.522E-3	9.089E-2
1.3E+7	5.578E-3	1.259E-1
1.2E+7	5.545E-3	1.603E-1
1.1E+7	5.410E-3	1.617E-1
1.0E+7	5.148E-3	1.411E-1
9.0E+6	4.861E-3	8.825E-2
8.0E+6	4.975E-3	1.073E-1
7.0E+6	6.042E-3	1.711E-1
6.0E+6	7.569E-3	1.065E-1
5.0E+6		

* Read as 4.4×10^7.

Table 15 Measured neutron spectra behind 0cm thick iron by the BC501A detector for 68-MeV p-Li neutrons.

Energy (eV)	Neutron Flux (n/cm^2/Lethargy/μC)	Error (%)	Neutron Flux (n/cm^2/Lethargy/μC)	Error (%)
	20 cm from beam axis		40 cm from beam axis	
7.0E+7*	3.691E+1	3.200E-2	1.843E+0	7.081E-2
6.8E+7	6.570E+1	4.425E-2	4.089E+0	8.662E-2
6.6E+7	8.288E+1	3.758E-2	5.266E+0	7.182E-2
6.4E+7	6.981E+1	4.223E-2	4.327E+0	8.281E-2
6.2E+7	4.212E+1	7.498E-2	3.137E+0	1.267E-1
6.0E+7	2.581E+1	8.884E-2	2.388E+0	1.220E-1
5.8E+7	2.372E+1	6.050E-2	1.965E+0	9.298E-2
5.6E+7	2.565E+1	6.772E-2	1.940E+0	1.143E-1
5.4E+7	2.754E+1	5.447E-2	2.286E+0	8.469E-2
5.2E+7	2.937E+1	5.686E-2	2.858E+0	7.519E-2
5.0E+7	3.290E+1	5.003E-2	3.180E+0	6.720E-2
4.8E+7	3.860E+1	5.731E-2	3.218E+0	9.295E-2
4.6E+7	3.852E+1	6.404E-2	3.359E+0	9.708E-2
4.4E+7	3.482E+1	7.234E-2	3.505E+0	9.332E-2
4.3E+7	3.283E+1	6.860E-2	3.554E+0	8.284E-2
4.2E+7	3.164E+1	5.866E-2	3.555E+0	7.004E-2
4.1E+7	3.080E+1	6.195E-2	3.532E+0	7.271E-2
4.0E+7	3.023E+1	6.927E-2	3.530E+0	8.048E-2
3.9E+7	3.037E+1	7.771E-2	3.586E+0	9.004E-2
3.8E+7	3.162E+1	8.004E-2	3.713E+0	9.405E-2
3.7E+7	3.376E+1	7.020E-2	3.883E-0	8.558E-2
3.6E+7	3.610E+1	5.435E-2	4.018E+0	7.008E-2
3.5E+7	3.808E+1	4.370E-2	4.030E+0	5.918E-2
3.4E+7	3.934E+1	3.930E-2	3.906E+0	5.530E-2
3.3E+7	3.911E+1	4.848E-2	3.744E+0	6.458E-2
3.2E+7	3.653E+1	6.597E-2	3.658E+0	8.024E-2
3.1E+7	3.234E+1	9.898E-2	3.667E+0	1.072E-1
3.0E+7	2.947E+1	1.017E-1	3.710E+0	1.015E-1
2.9E+7	3.028E+1	5.026E-2	3.740E+0	5.631E-2
2.8E+7	3.327E+1	6.658E-2	3.757E+0	7.620E-2
2.7E+7	3.456E+1	4.569E-2	3.752E+0	5.784E-2
2.6E+7	3.282E+1	9.842E-2	3.700E+0	1.012E-1
2.5E+7	3.013E+1	1.448E-1	3.604E+0	1.356E-1
2.4E+7	2.822E+1	1.217E-1	3.471E+0	1.110E-1
2.3E+7	2.685E+1	7.724E-2	3.291E+0	7.274E-2
2.2E+7	2.539E+1	5.404E-2	3.138E+0	5.440E-2
2.1E+7	2.370E+1	3.760E-2	3.127E+0	4.017E-2
2.0E+7	2.173E+1	5.357E-2	3.202E+0	4.794E-2
1.9E+7	1.992E+1	1.135E-1	3.211E+0	8.328E-2
1.8E+7	1.883E+1	1.620E-1	3.125E+0	1.105E-1
1.7E+7	1.814E+1	1.254E-1	2.964E+0	9.143E-2
1.6E+7	1.745E+1	8.126E-2	2.783E+0	6.608E-2
1.5E+7	1.736E+1	1.313E-1	2.690E+0	9.528E-2
1.4E+7	1.821E+1	5.859E-2	2.709E+0	4.913E-2
1.3E+7	1.864E+1	8.069E-2	2.809E+0	6.394E-2
1.2E+7	1.823E+1	7.778E-2	2.924E+0	5.431E-2
1.1E+7	1.862E+1	4.722E-2	2.935E+0	3.526E-2
1.0E+7	1.792E+1	3.421E-2	2.821E+0	2.811E-2
9.0E+6	1.244E+1	7.667E-2	2.274E+0	5.822E-2
8.0E+6				

* Read as 7.0×10^7.

Table 16 Measured neutron spectra behind 20cm thick iron by the BC501A detector for 68-MeV p-Li neutrons.

Energy (eV)	Neutron Flux (n/cm^2/Lethargy/μC)	Error (%)	Neutron Flux (n/cm^2/Lethargy/μC)	Error (%)	Neutron Flux (n/cm^2/Lethargy/μC)	Error (%)
	beam axis		20 cm from beam axis		40 cm from beam axis	
7.0E+7*			1.376E+2	5.005E-2	5.767E+0	8.427E-2
6.8E+7	1.749E+4	5.312E-2	2.939E+2	7.057E-2	1.032E+1	1.398E-1
6.6E+7	3.935E+4	3.299E-2	3.935E+2	4.732E-2	1.636E+1	8.032E-2
6.4E+7	2.948E+4	4.966E-2	3.389E+2	3.821E-2	1.803E+1	5.068E-2
6.2E+7	1.329E+4	9.676E-2	2.336E+2	1.018E-1	1.340E+1	1.287E-1
6.0E+7	3.507E+3	1.807E-1	1.564E+2	1.090E-1	8.997E+0	1.375E-1
5.8E+7	8.566E+2	4.206E-1	1.172E+2	3.489E-2	8.150E+0	3.616E-2
5.6E+7	1.883E+3	1.568E-1	1.144E+2	6.611E-2	8.923E+0	6.218E-2
5.4E+7	2.953E+3	5.848E-2	1.278E+2	5.056E-2	9.937E+0	4.823E-2
5.2E+7	3.628E+3	3.933E-2	1.426E+2	3.504E-2	1.096E+1	3.506E-2
5.0E+7	4.020E+3	3.978E-2	1.539E+2	3.000E-2	1.191E+1	3.118E-2
4.8E+7	4.115E+3	4.571E-2	1.605E+2	2.795E-2	1.264E+1	2.923E-2
4.6E+7	3.835E+3	4.850E-2	1.621E+2	2.509E-2	1.311E+1	2.544E-2
4.4E+7	3.483E+3	5.240E-2	1.606E+2	2.380E-2	1.333E+1	2.302E-2
4.3E+7	3.264E+3	5.441E-2	1.586E+2	2.424E-2	1.345E+1	2.269E-2
4.2E+7	3.088E+3	5.531E-2	1.562E+2	2.595E-2	1.358E+1	2.370E-2
4.1E+7	2.948E+3	6.113E-2	1.538E+2	2.911E-2	1.370E+1	2.621E-2
4.0E+7	2.829E+3	7.055E-2	1.517E+2	3.375E-2	1.385E+1	3.016E-2
3.9E+7	2.735E+3	7.846E-2	1.498E+2	3.749E-2	1.399E+1	3.322E-2
3.8E+7	2.679E+3	8.119E-2	1.483E+2	3.988E-2	1.413E+1	3.507E-2
3.7E+7	2.663E+3	7.691E-2	1.469E+2	4.110E-2	1.423E+1	3.594E-2
3.6E+7	2.664E+3	6.813E-2	1.454E+2	4.149E-2	1.427E+1	3.624E-2
3.5E+7	2.647E+3	6.060E-2	1.434E+2	4.158E-2	1.424E+1	3.626E-2
3.4E+7	2.578E+3	5.997E-2	1.409E+2	4.152E-2	1.411E+1	3.624E-2
3.3E+7	2.445E+3	6.883E-2	1.376E+2	4.137E-2	1.388E+1	3.612E-2
3.2E+7	2.263E+3	8.546E-2	1.337E+2	4.102E-2	1.358E+1	3.572E-2
3.1E+7	2.080E+3	9.707E-2	1.292E+2	4.084E-2	1.323E+1	3.540E-2
3.0E+7	1.963E+3	8.701E-2	1.244E+2	4.172E-2	1.287E+1	3.600E-2
2.9E+7	1.947E+3	6.543E-2	1.193E+2	4.490E-2	1.252E+1	3.854E-2
2.8E+7	1.988E+3	6.308E-2	1.140E+2	5.104E-2	1.217E+1	4.354E-2
2.7E+7	1.975E+3	8.678E-2	1.086E+2	5.937E-2	1.182E+1	5.016E-2
2.6E+7	1.824E+3	1.309E-1	1.033E+2	6.730E-2	1.147E+1	5.613E-2
2.5E+7	1.561E+3	1.793E-1	9.800E+1	7.164E-2	1.110E+1	5.862E-2
2.4E+7	1.304E+3	2.000E-1	9.295E+1	6.883E-2	1.071E+1	5.527E-2
2.3E+7	1.142E+3	1.731E-1	8.823E+1	5.734E-2	1.029E+1	4.512E-2
2.2E+7	1.056E+3	1.171E-1	8.388E+1	3.841E-2	9.843E+0	2.944E-2
2.1E+7	9.670E+2	5.690E-2	7.989E+1	1.775E-2	9.382E+0	1.271E-2
2.0E+7	8.446E+2	1.332E-1	7.616E+1	3.214E-2	8.930E+0	2.452E-2
1.9E+7	7.355E+2	2.568E-1	7.256E+1	4.673E-2	8.516E+0	3.621E-2
1.8E+7	6.860E+2	3.009E-1	6.902E+1	4.926E-2	8.169E+0	3.763E-2
1.7E+7	6.658E+2	2.128E-1	6.569E+1	4.001E-2	7.902E+0	2.970E-2
1.6E+7	6.159E+2	1.332E-1	6.289E+1	2.641E-2	7.715E+0	1.905E-2
1.5E+7	5.428E+2	1.799E-1	6.089E+1	1.836E-2	7.589E+0	1.322E-2
1.4E+7	4.990E+2	8.499E-2	5.961E+1	2.177E-2	7.490E+0	1.597E-2
1.3E+7	4.958E+2	1.506E-1	5.852E+1	3.291E-2	7.370E+0	2.433E-2
1.2E+7	5.013E+2	1.966E-1	5.659E+1	4.151E-2	7.126E+0	3.101E-2
1.1E+7	4.957E+2	1.654E-1	5.244E+1	4.710E-2	6.580E+0	3.530E-2
1.0E+7	4.740E+2	1.214E-1	4.491E+1	5.959E-2	5.575E+0	4.393E-2
9.0E+6	4.025E+2	1.055E-1	3.411E+1	8.033E-2	4.155E+0	5.909E-2
8.0E+6	2.624E+2	1.631E-1				
7.0E+6						

* Read as 7.0×10^7.

Table 17 Measured neutron spectra behind 40cm thick iron by the BC501A detector for 68-MeV p-Li neutrons.

Energy (eV)	Neutron Flux (n/cm²/Lethargy/μC)	Error (%)	Neutron Flux (n/cm²/Lethargy/μC)	Error (%)	Neutron Flux (n/cm²/Lethargy/μC)	Error (%)
	beam axis		20 cm from beam axis		40 cm from beam axis	
7.0E+7*			2.495E+1	1.384E-1	3.943E+0	1.311E-1
6.8E+7	1.317E+3	8.626E-2	1.429E+2	8.502E-2	8.470E+0	2.613E-1
6.6E+7	3.213E+3	4.896E-2	2.908E+2	5.873E-2	1.838E+1	1.612E-1
6.4E+7	2.691E+3	6.730E-2	2.426E-2	8.487E-2	2.103E+1	1.403E-1
6.2E+7	1.069E+3	1.496E-1	1.739E+2	1.207E-1	9.624E+0	3.540E-1
6.0E+7	2.624E+2	3.008E-1	7.527E+1	1.318E-1	4.867E+0	3.450E-1
5.8E+7	1.533E+2	2.934E-1	3.027E+1	1.922E-1	5.586E+0	1.178E-1
5.6E+7	2.234E+2	1.640E-1	3.824E+1	1.222E-1	6.091E+0	1.130E-1
5.4E+7	2.779E+2	7.589E-2	4.967E+1	5.404E-2	6.463E+0	7.303E-2
5.2E+7	3.067E+2	5.611E-2	5.700E+1	4.065E-2	6.775E+0	5.169E-2
5.0E+7	3.230E+2	5.957E-2	6.067E+1	4.340E-2	6.971E+0	4.600E-2
4.8E+7	3.219E+2	6.965E-2	6.162E+1	5.049E-2	7.000E+0	4.433E-2
4.6E+7	2.959E+2	7.435E-2	5.953E+1	5.218E-2	6.866E+0	4.107E-2
4.4E+7	2.696E+2	8.049E-2	5.639E+1	5.293E-2	6.701E+0	4.013E-2
4.3E+7	2.547E+2	8.386E-2	5.425E+1	5.268E-2	6.579E+0	4.183E-2
4.2E+7	2.429E+2	8.621E-2	5.262E+1	5.272E-2	6.456E+0	4.586E-2
4.1E+7	2.323E+2	9.483E-2	5.160E+1	5.795E-2	6.339E+0	5.193E-2
4.0E+7	2.213E+2	1.093E-1	5.104E+1	6.638E-2	6.228E+0	5.944E-2
3.9E+7	2.111E+2	1.230E-1	5.060E+1	7.322E-2	6.123E+0	6.539E-2
3.8E+7	2.047E+2	1.290E-1	4.997E+1	7.605E-2	6.020E+0	6.907E-2
3.7E+7	2.042E+2	1.222E-1	4.891E+1	7.381E-2	5.911E+0	7.050E-2
3.6E+7	2.078E+2	1.060E-1	4.731E+1	6.785E-2	5.790E+0	7.022E-2
3.5E+7	2.103E+2	9.006E-2	4.523E+1	6.177E-2	5.650E+0	6.908E-2
3.4E+7	2.063E+2	8.405E-2	4.291E+1	6.052E-2	5.493E+0	6.760E-2
3.3E+7	1.947E-2	9.132E-2	4.057E+1	6.670E-2	5.326E+0	6.590E-2
3.2E+7	1.792E+2	1.108E-1	3.826E+1	7.906E-2	5.158E+0	6.378E-2
3.1E+7	1.663E+2	1.257E-1	3.597E+1	8.688E-2	4.995E+0	6.144E-2
3.0E+7	1.607E+2	1.126E-1	3.381E+1	7.835E-2	4.836E+0	5.990E-2
2.9E+7	1.621E+2	8.569E-2	3.208E+1	6.250E-2	4.671E+0	6.067E-2
2.8E+7	1.651E+2	8.153E-2	3.096E+1	6.363E-2	4.487E+0	6.468E-2
2.7E+7	1.628E+2	1.042E-1	3.007E+1	8.623E-2	4.280E+0	7.147E-2
2.6E+7	1.518E+2	1.455E-1	2.874E+1	1.207E-1	4.055E+0	7.889E-2
2.5E+7	1.348E+2	1.890E-1	2.670E+1	1.499E-1	3.826E+0	8.327E-2
2.4E+7	1.192E+2	2.001E-1	2.430E+1	1.526E-1	3.604E+0	8.074E-2
2.3E+7	1.108E+2	1.674E-1	2.212E+1	1.279E-1	3.396E+0	6.932E-2
2.2E+7	1.081E+2	1.154E-1	2.043E+1	9.109E-2	3.196E+0	5.047E-2
2.1E+7	1.030E+2	6.590E-2	1.914E+1	4.989E-2	2.996E+0	2.963E-2
2.0E+7	8.995E+1	1.288E-1	1.807E+1	9.281E-2	2.793E+0	4.869E-2
1.9E+7	7.298E+1	2.472E-1	1.713E+1	1.551E-1	2.601E+0	6.940E-2
1.8E+7	6.101E+1	3.224E-1	1.633E+1	1.794E-1	2.446E+0	7.629E-2
1.7E+7	5.711E+1	2.555E-1	1.565E+1	1.373E-1	2.355E+0	6.599E-2
1.6E+7	5.636E+1	1.638E-1	1.488E+1	9.483E-2	2.332E+0	4.618E-2
1.5E+7	5.490E+1	1.708E-1	1.398E+1	1.098E-1	2.350E+0	3.108E-2
1.4E+7	5.364E+1	8.348E-2	1.331E+1	5.679E-2	2.367E+0	3.058E-2
1.3E+7	5.355E+1	1.338E-1	1.309E+1	9.228E-2	2.359E+0	4.148E-2
1.2E+7	5.443E+1	1.593E-1	1.300E+1	1.102E-1	2.330E+0	5.099E-2
1.1E+7	5.643E+1	1.302E-1	1.276E+1	9.514E-2	2.307E+0	5.180E-2
1.0E+7	5.988E+1	9.310E-2	1.293E+1	7.193E-2	2.332E+0	4.010E-2
9.0E+6	6.519E+1	5.990E-2	1.401E+1	4.449E-2	2.448E+0	1.561E-2
8.0E+6	6.986E+1	4.127E-2	1.577E+1	2.966E-2	2.665E+0	2.846E-2
7.0E+6	6.517E+1	2.338E-1				
6.0E+6						

* Read as 7.0×10^7.

Table 18 Measured neutron spectrum behind 70cm thick iron by the BC501A detector for 68-MeV p-Li neutrons.

Energy (eV)	Neutron Flux (n/cm^2/Lethargy/μC)	Error (%)
	beam axis	
6.8E+7*	3.004E+1	1.267E-1
6.6E+7	7.445E+1	6.931E-2
6.4E+7	6.989E+1	8.917E-2
6.2E+7	4.354E+1	1.287E-1
6.0E+7	1.313E+1	2.118E-1
5.8E+7	2.172E+0	7.261E-1
5.6E+7	4.401E+0	2.918E-1
5.4E+7	6.914E+0	1.051E-1
5.2E+7	8.521E+0	6.888E-2
5.0E+7	9.587E+0	6.895E-2
4.8E+7	9.459E+0	8.135E-2
4.6E+7	7.932E+0	9.450E-2
4.4E+7	6.724E+0	1.098E-1
4.3E+7	6.325E+0	1.156E-1
4.2E+7	6.244E+0	1.162E-1
4.1E+7	6.282E+0	1.219E-1
4.0E+7	6.227E+0	1.348E-1
3.9E+7	6.001E+0	1.503E-1
3.8E+7	5.695E+0	1.615E-1
3.7E+7	5.453E+0	1.597E-1
3.6E+7	5.329E+0	1.440E-1
3.5E+7	5.245E+0	1.244E-1
3.4E+7	5.064E+0	1.145E-1
3.3E+7	4.734E+0	1.214E-1
3.2E+7	4.363E+0	1.450E-1
3.1E+7	4.166E+0	1.612E-1
3.0E+7	4.306E+0	1.375E-1
2.9E+7	4.717E+0	9.828E-2
2.8E+7	5.089E+0	8.721E-2
2.7E+7	5.055E+0	1.046E-1
2.6E+7	4.481E+0	1.454E-1
2.5E+7	3.618E+0	2.026E-1
2.4E+7	2.912E+0	2.325E-1
2.3E+7	2.650E+0	1.976E-1
2.2E+7	2.748E+0	1.312E-1
2.1E+7	2.878E+0	7.512E-2
2.0E+7	2.784E+0	1.281E-1
1.9E+7	2.482E+0	2.177E-1
1.8E+7	2.175E+0	2.715E-1
1.7E+7	2.008E+0	2.299E-1
1.6E+7	1.965E+0	1.574E-1
1.5E+7	1.975E+0	1.432E-1
1.4E+7	1.978E+0	7.331E-2
1.3E+7	1.942E+0	1.114E-1
1.2E+7	1.929E+0	1.278E-1
1.1E+7	1.987E+0	1.069E-1
1.0E+7	2.077E+0	8.093E-2
9.0E+6	2.176E+0	6.135E-2
8.0E+6	2.145E+0	1.076E-1
7.0E+6	1.668E+0	1.927E-1
6.0E+6		

* Read as 6.8×10^7.

Table 19 Measured neutron spectrum behind 100cm thick iron by the BC501A detector for 68-MeV p-Li neutrons.

Energy (eV)	Neutron Flux (n/cm^2/Lethargy/μC)	Error (%)
	beam axis	
6.8E+7*	8.067E-1	1.765E-1
6.6E+7	2.274E+0	7.792E-2
6.4E+7	2.575E+0	1.088E-1
6.2E+7	1.569E+0	1.845E-1
6.0E+7	4.566E-1	3.145E-1
5.8E+7	1.357E-1	5.962E-1
5.6E+7	2.211E-1	2.882E-1
5.4E+7	3.154E-1	1.107E-1
5.2E+7	3.732E-1	7.931E-2
5.0E+7	3.992E-1	8.479E-2
4.8E+7	3.760E-1	1.047E-1
4.6E+7	2.999E-1	1.295E-1
4.4E+7	2.416E-1	1.555E-1
4.3E+7	2.200E-1	1.650E-1
4.2E+7	2.139E-1	1.680E-1
4.1E+7	2.178E-1	1.773E-1
4.0E+7	2.243E-1	1.930E-1
3.9E+7	2.280E-1	2.076E-1
3.8E+7	2.267E-1	2.151E-1
3.7E+7	2.207E-1	2.105E-1
3.6E+7	2.116E-1	1.936E-1
3.5E+7	2.009E-1	1.714E-1
3.4E+7	1.884E-1	1.571E-1
3.3E+7	1.731E-1	1.626E-1
3.2E+7	1.559E-1	1.947E-1
3.1E+7	1.432E-1	2.235E-1
3.0E+7	1.439E-1	1.962E-1
2.9E+7	1.598E-1	1.408E-1
2.8E+7	1.794E-1	1.202E-1
2.7E+7	1.855E-1	1.305E-1
2.6E+7	1.702E-1	1.646E-1
2.5E+7	1.423E-1	2.162E-1
2.4E+7	1.190E-1	2.376E-1
2.3E+7	1.097E-1	2.002E-1
2.2E+7	1.107E-1	1.433E-1
2.1E+7	1.124E-1	9.706E-2
2.0E+7	1.092E-1	1.539E-1
1.9E+7	1.017E-1	2.409E-1
1.8E+7	9.315E-2	2.875E-1
1.7E+7	8.674E-2	2.546E-1
1.6E+7	8.479E-2	1.820E-1
1.5E+7	8.782E-2	1.426E-1
1.4E+7	9.208E-2	7.779E-2
1.3E+7	9.242E-2	1.044E-1
1.2E+7	9.001E-2	1.123E-1
1.1E+7	9.085E-2	9.821E-2
1.0E+7	9.638E-2	7.779E-2
9.0E+6	1.014E-1	5.621E-2
8.0E+6	9.507E-2	1.058E-1
7.0E+6	6.833E-2	2.138E-1
6.0E+6		

* Read as 6.8×10^7.

Table 20 Measured neutron spectrum behind 130cm thick iron by the BC501A detector for 68-MeV p-Li neutrons.

Energy (eV)	Neutron Flux (n/cm²/Lethargy/μC)	Error (%)
	beam axis	
6.8E+7	5.212E-2	3.342E-1
6.6E+7	1.167E-1	1.963E-1
6.4E+7	7.148E-2	4.194E-1
6.2E+7	6.278E-2	4.492E-1
6.0E+7	2.871E-2	4.852E-1
5.8E+7	5.186E-3	1.554E+0
5.6E+7	7.440E-3	8.801E-1
5.4E+7	1.033E-2	3.510E-1
5.2E+7	1.160E-2	2.460E-1
5.0E+7	1.232E-2	2.627E-1
4.8E+7	1.377E-2	2.752E-1
4.6E+7	1.623E-2	2.276E-1
4.4E+7	1.745E-2	2.079E-1
4.3E+7	1.728E-2	2.089E-1
4.2E+7	1.626E-2	2.254E-1
4.1E+7	1.465E-2	2.655E-1
4.0E+7	1.289E-2	3.303E-1
3.9E+7	1.150E-2	3.997E-1
3.8E+7	1.076E-2	4.388E-1
3.7E+7	1.051E-2	4.285E-1
3.6E+7	1.033E-2	3.834E-1
3.5E+7	9.920E-3	3.310E-1
3.4E+7	9.407E-3	2.903E-1
3.3E+7	9.112E-3	2.718E-1
3.2E+7	9.078E-3	2.855E-1
3.1E+7	8.974E-3	3.082E-1
3.0E+7	8.525E-3	2.967E-1
2.9E+7	7.876E-3	2.633E-1
2.8E+7	7.378E-3	2.605E-1
2.7E+7	7.075E-3	2.735E-1
2.6E+7	6.642E-3	3.035E-1
2.5E+7	5.890E-3	3.616E-1
2.4E+7	5.098E-3	3.786E-1
2.3E+7	4.689E-3	3.225E-1
2.2E+7	4.656E-3	2.521E-1
2.1E+7	4.568E-3	2.135E-1
2.0E+7	4.193E-3	3.308E-1
1.9E+7	3.917E-3	4.835E-1
1.8E+7	4.230E-3	4.894E-1
1.7E+7	4.901E-3	3.862E-1
1.6E+7	5.218E-3	2.811E-1
1.5E+7	4.952E-3	1.991E-1
1.4E+7	4.395E-3	1.440E-1
1.3E+7	3.901E-3	1.938E-1
1.2E+7	3.829E-3	1.803E-1
1.1E+7	4.140E-3	1.524E-1
1.0E+7	4.481E-3	1.288E-1
9.0E+6	4.933E-3	7.580E-2
8.0E+6	5.620E-3	7.463E-2
7.0E+6	6.255E-3	1.121E-1
6.0E+6		

* Read as 6.8×10^7.

Table 21 Measured reaction rates behind iron by the Bonner ball counter for 43-MeV p-Li neutrons.

Counter	Reaction rate (n/μC)	Reaction rate (n/μC)	Reaction rate (n/μC)
	20 cm thick	40 cm thick	100 cm thick
Bare	1.08170E+03*	2.32029E+02	2.29024E+01
1.5cm	7.70767E+03	3.09448E+03	1.85478E+02
3.0cm	2.13367E+04	7.54156E+03	3.94076E+02
5.0cm	2.27974E+04	9.20984E+03	4.71565E+02
9.0cm	1.78810E+04	4.56463E+03	1.59767E+02

* Read as 1.08170×10^{3}.

Table 22 Measured reaction rates behind iron by the Bonner ball counter for 68-MeV p-Li neutrons.

Counter	Reaction rate (n/μC)	Reaction rate (n/μC)	Reaction rate (n/μC)
	20 cm thick	40 cm thick	100 cm thick
Bare	9.20495E+02*	4.94764E+02	7.23828E+01
1.5cm	1.08745E+04	7.58654E+03	6.28653E+02
3.0cm	3.31695E+04	1.85827E+04	1.30211E+03
5.0cm	5.13089E+04	2.24907E+04	1.34292E+03
9.0cm	3.84652E+04	1.34443E+04	5.40227E+02

* Read as 9.20495×10^{2}.

Table 23 Measured neutron spectra behind iron by the Bonner ball counter for 43-MeV p-Li neutrons.

Energy (eV)	Neutron Flux (n/cm^2/Lethargy/μC)	Neutron Flux (n/cm^2/Lethargy/μC)	Neutron Flux (n/cm^2/Lethargy/μC)
	20cm thick	40cm thick	100cm thick
4.500E+07*	2.740E+03	9.760E+01	8.940E-02
3.500E+07	6.395E+02	2.277E+01	5.349E-02
2.750E+07	5.945E+02	2.677E+01	1.415E-02
2.250E+07	4.454E+02	1.203E+01	5.843E-03
1.750E+07	3.016E+02	1.088E+01	5.141E-03
1.350E+07	2.027E+02	6.209E+00	1.069E-02
1.000E+07	1.245E+02	4.294E+00	7.898E-03
6.700E+06	1.316E+02	5.434E+00	1.549E-02
4.490E+06	1.753E+02	1.629E-01	7.986E-02
3.010E+06	2.725E+02	2.354E+01	6.793E-02
2.020E+06	3.424E+02	5.151E+01	1.369E-01
1.350E+06	4.830E+02	8.128E+01	2.440E-01
9.070E+05	7.111E+02	1.965E-02	3.249E+00
4.980E+05	8.604E+02	3.787E+02	1.147E+01
2.240E+05	4.851E+02	2.073E+02	9.915E+00
8.650E+04	2.700E+02	1.570E+02	1.200E+01
1.500E+04	4.618E+01	1.798E+01	1.015E+00
3.350E+03	2.620E+01	1.238E+01	8.151E-01
4.540E+02	2.930E+01	3.361E+00	1.190E+00
2.260E+01	1.769E+01	3.892E+00	6.792E-01
5.040E+00	8.083E+00	1.233E+00	4.982E-02
1.120E+00	5.673E+00	1.036E+00	2.216E-01
4.140E-01	3.083E+00	6.747E-01	3.199E-02
1.000E-04			

* Read as 4.500×10^7.

Table 24 Measured neutron spectra behind iron by the Bonner ball counter for 68-MeV p-Li neutrons.

Energy (eV)	Neutron Flux (n/cm^2/Lethargy/μC)	Neutron Flux (n/cm^2/Lethargy/μC)	Neutron Flux (n/cm^2/Lethargy/μC)
	20cm thick	40cm thick	100cm thick
8.000E+07*	1.190E+03	1.752E+02	5.770E+00
6.500E+07	6.935E+03	9.746E+02	1.593E+01
5.500E+07	2.458E+03	2.874E+02	3.469E+00
4.500E+07	1.866E+03	2.185E+02	4.852E+00
3.500E+07	1.345E+03	1.310E+02	2.727E+00
2.750E+07	8.752E+02	1.051E+02	4.563E+00
2.250E+07	5.086E+02	4.134E+01	1.570E+00
1.750E+07	4.332E+02	5.888E+01	8.451E-01
1.350E+07	2.940E+02	3.836E+01	2.413E+00
1.000E+07	2.683E+02	4.429E+01	6.809E-01
6.700E+06	3.227E+02	4.553E+01	4.022E-01
4.490E+06	5.317E+02	6.325E+01	7.252E-01
3.010E+06	7.730E+02	1.312E+02	1.394E+00
2.020E+06	1.032E+03	1.754E+02	1.894E+00
1.350E+06	1.471E+03	3.185E+02	2.629E+00
9.070E+05	1.937E+03	6.238E+02	9.968E+00
4.980E+05	1.776E+03	9.477E+02	3.244E+01
2.240E+05	7.556E+02	5.293E+02	2.462E+01
8.650E+04	2.506E+02	2.938E+02	4.171E+01
1.500E+04	3.540E+01	4.733E+01	5.577E+00
3.350E+03	2.018E+01	3.383E+01	4.850E+00
4.540E+02	1.072E+01	1.424E+01	2.132E+00
2.260E+01	4.297E+00	5.617E+00	1.515E+00
5.040E+00	3.210E+00	3.107E+00	4.835E-01
1.120E+00	3.045E+00	2.191E+00	2.606E-01
4.140E-01	3.437E+00	1.201E+00	1.855E-01
1.000E-04			

* Read as 8.000×10^7.

Table 25 Measured fission reaction rates of ^{238}U and ^{232}Th for 43-MeV p-Li neutrons.

Position Z[a] (cm)	Position R[b] (cm)	Fission reaction rate ^{238}U (n/μC)	(%)	^{232}Th (n/μC)	(%)
0	0	8.01E+4[c]	(0.59)	3.27E+4	(0.24)
10	0	2.43E+4	(1.00)	1.02E+4	(0.89)
20	0	5.64E+3	(1.81)	2.49E+3	(0.99)
40	0	2.97E+2	(3.43)	1.16E+2	(3.34)
70	0	6.96E+0	(9.76)	1.79E+0	(27.7)
0	20	1.00E+2	(4.30)		
10	20	2.47E+2	(5.74)		
20	20	1.95E+2	(3.53)	6.12E+1	(17.4)
40	20	5.14E+1	(5.02)	1.77E+1	(14.0)
70	20	3.61E+0	(19.6)	1.53E+0	(20.9)

[a] Thichness of iron shields.
[b] Distance from the beam axis.
[c] Read as 8.01×10^4.

Table 26 Measured fission reaction rates of ^{238}U and ^{232}Th for 68-MeV p-Li neutrons.

Position Z[a] (cm)	Position R[b] (cm)	Fission reaction rate ^{238}U (n/μC)	(%)	^{232}Th (n/μC)	(%)
0	0	1.18E+5[c]	(0.38)	5.71E+4	(0.49)
20	0	1.53E+4	(0.66)	7.70E+3	(0.90)
40	0	1.23E+3	(2.26)	5.47E+2	(3.28)
70	0	3.18E+1	(7.14)	1.08E+1	(11.9)
100	0	2.59E+0	(11.0)	8.51E-1	(18.6)
20	20	7.14E+1	(3.96)	4.69E+1	(4.73)
40	20	1.68E+2	(3.41)	1.15E+2	(4.01)
70	20	1.58E+1	(5.95)	7.12E+0	(8.61)
100	20	2.57E+0	(9.25)	9.07E-1	(15.1)
130	20	1.08E+0	(11.9)	4.59E-1	(17.7)

[a] Thichness of iron shields.
[b] Distance from the beam axis.
[c] Read as 1.18×10^5.

Table 27 Difference of neutron reaction rates of ^{7}LiF and ^{nat}LiF TLDs for 43- and 68-MeV p-Li neutrons.

Position[a] (cm)	Difference of reaction rate (^{60}Coeq. R/μC)	(%)	(^{60}Coeq. R/μC)	(%)
	43 MeV		68 MeV	
40	2.60E-7[b]	63.2	1.07E-6	40.2
70	1.58E-7	12.2	3.68E-7	10.3
100	3.59E-7	8.8	1.30E-7	15.1
130			2.66E-7	12.1

[a] Thichness of iron shields.
[b] Read as 2.60 x 10^{-7}.

Table 28 Measured neutron reaction rates using solid state nuclear track detector for 43- and 68-MeV p-Li neutrons.

Position[a] (cm)	Reaction rate (Pits/cm^2/μC)	(%)	(Pits/cm^2/μC)	(%)
	43 MeV		68 MeV	
0	3.99E+1[b]	5.6		
10	1.83E+1	6.2		
20	6.23E+0	5.5	1.64E+1	5.4
40	9.21E-1	7.9	3.29E+0	5.5
70	1.16E-1	8.1	5.19E-1	6.1
100	2.00E-2	16.0	8.63E-2	8.9
130			8.35E-3	24.1

[a] Thichness of iron shields.
[b] Read as 3.99 x 10^{1}.

Table 29 Measured neutron reaction rates using a rem counter made by Fuji Co. Ltd. for 43- and 68-MeV p-Li neutrons.

Position[a] (cm)	Reaction rate (μSv/μC) (%)	Position (cm)	Reaction rate (μSv/μC) (%)
	43 MeV		68 MeV
0	4.23E+0[b] (0.50)	0	4.58E+0 (0.45)
10	1.62E+0 (0.32)	20	1.52E+0 (0.28)
20	7.41E-1 (0.35)	40	4.60E-1 (0.41)
40	1.98E-1 (0.38)	70	9.06E-2 (0.62)
70	3.33E-2 (0.31)	100	1.93E-2 (0.76)
100	7.07E-3 (0.32)	130	4.06E-3 (0.45)

[a] Thichness of iron shields.
[b] Read as 4.23 x 10^{0}.

Table 30 Measured neutron reaction rates using the BC501A and Bonner ball detector for 43- and 68-MeV p-Li neutrons.

Position[a] (cm)	Reaction rate (μSv/μC)	Position (cm)	Reaction rate (μSv/μC)
	43 MeV		68 MeV
20	1.30	20	3.09
40	1.60E-1[b]	40	5.29E-1
100	3.25E-3	100	1.60E-2

[a] Thichness of iron shields.
[b] Read as 1.60 x 10^{-1}.

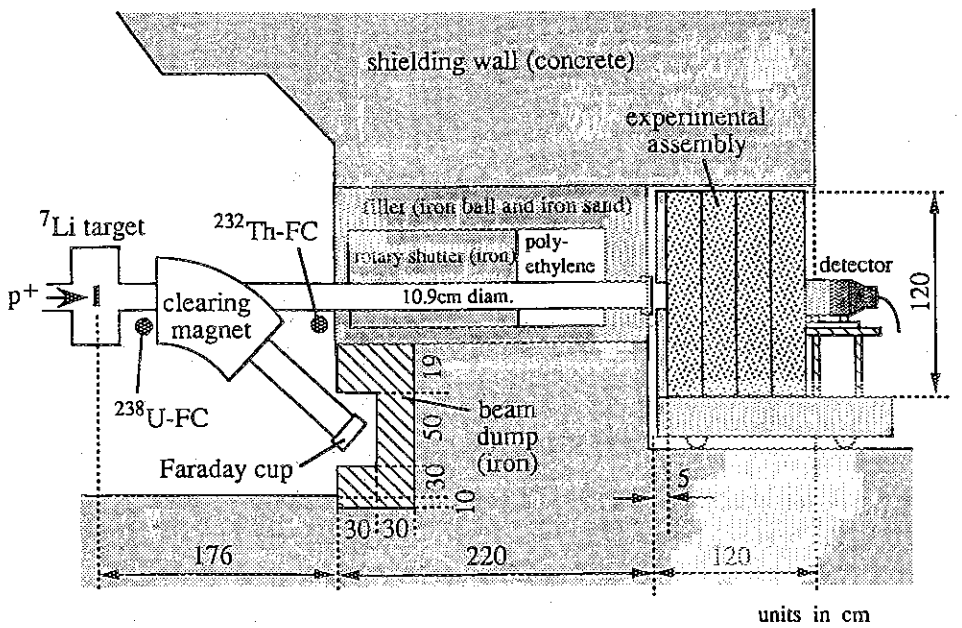

Fig. 1 Cross sectional view of the TIARA facility with the experimental arrangement.

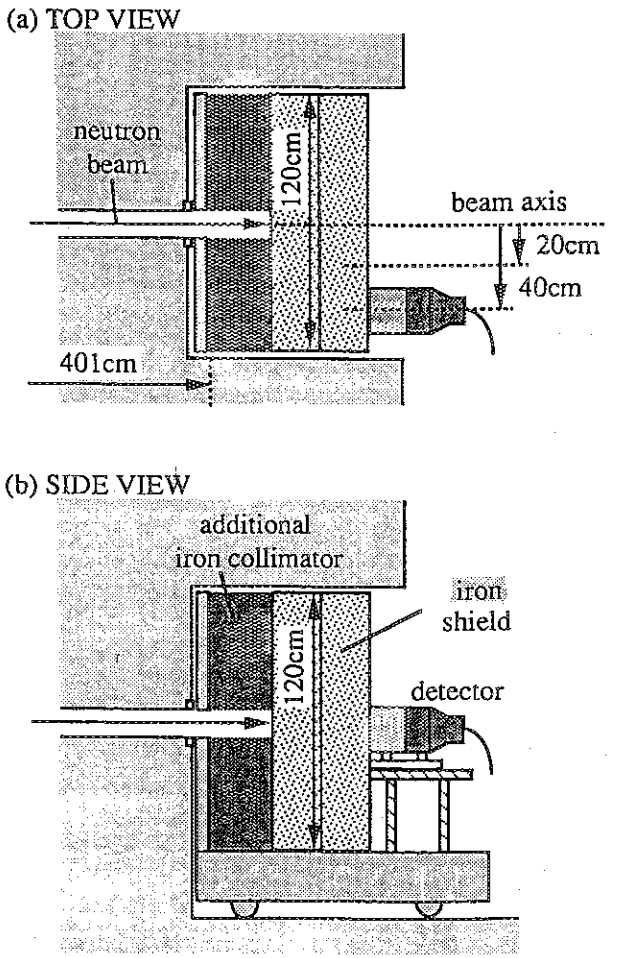

Fig. 2 Top view and side view of experimental arrangement for the iron shield with additional iron collimator.

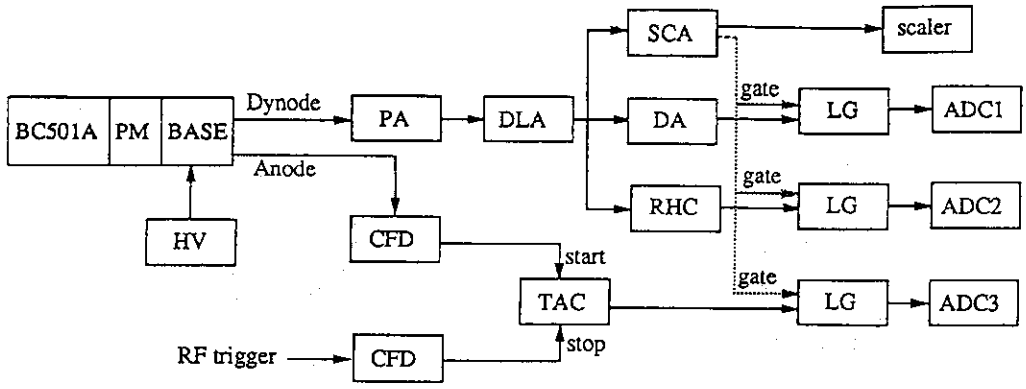

Fig. 3 Block diagram of the electronic circuits. PA:pre-amplifier, DLA: delay line amplifier, SCA: timing single channel analyzer, DA: delay amplifier, RHC: rise-time-to-pulse-height converter, CFD: constant fraction discriminator, TAC: time-to-amplitude converter, LG:linear gate stretcher, ADC: analog-to-digital converter. The scaler was used for counting the number of real events from the detector in order to estimate the counting loss.

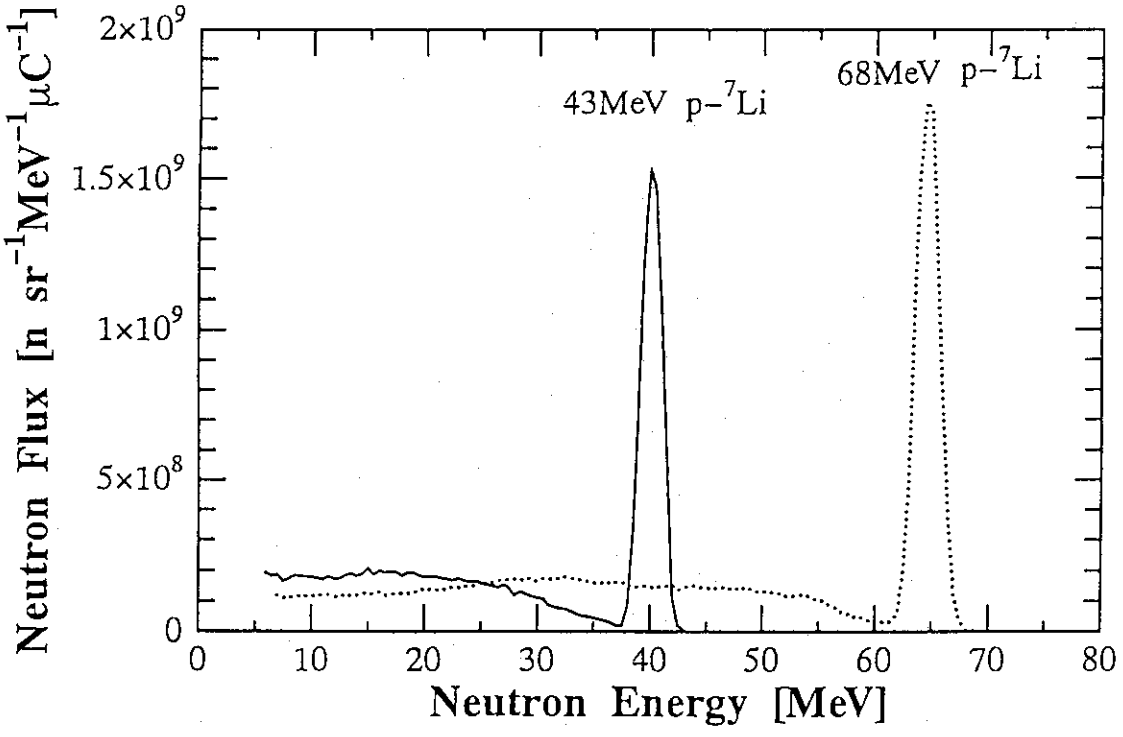

Fig. 4 Source neutron spectra generated via the ^{7}Li(p, n)reaction by 43- and 68-MeV protons. The spectra were measured by the time-of flight methods with the BC501A scintillation counter and absolutely normalized by the measurements using the recoil-proton counter telescope.

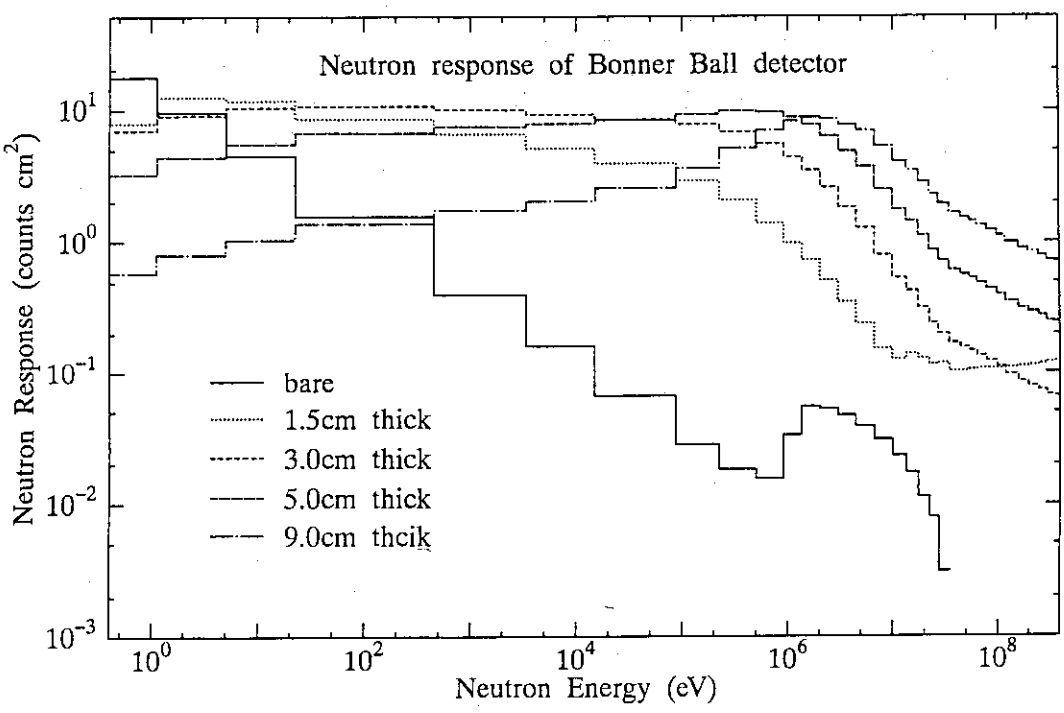

Fig. 5 Neutron responses of the Bonner ball counter for each moderator thickness: bare, 1.5, 3.0, and 9.0 cm. The almost responses were calculated by Uwamino et al. from adjoint calculations using the ANISN code except for the detector with 1.5-cm thick moderator. The response for the detector with 1.5-cm thick moderator was estimated by Ishikawa et al.

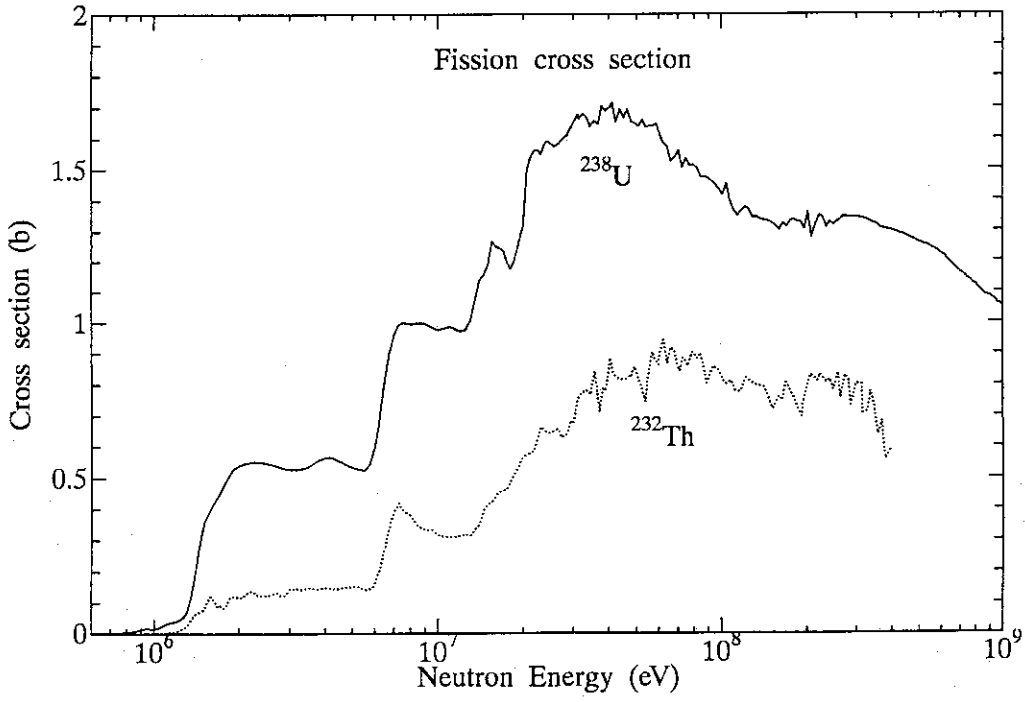

Fig. 6 Fission cross sections of ^{238}U and ^{232}Th. The cross sections up to 20 MeV is taken from JENDL-3, the cross sections between 20 and 400 MeV have been measured by Lisowski et al., and above 400 MeV have been calculated by him using the HETC code.

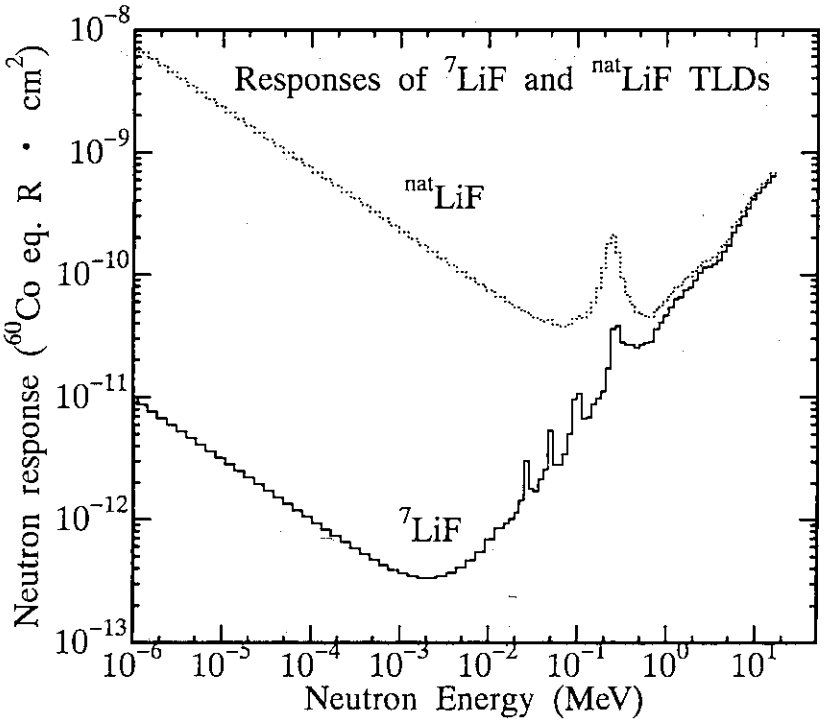

Fig. 7 Calculated neutron responses of ^{7}LiF and ^{nat}LiF TLDs using a code developed by Hashikura et al.

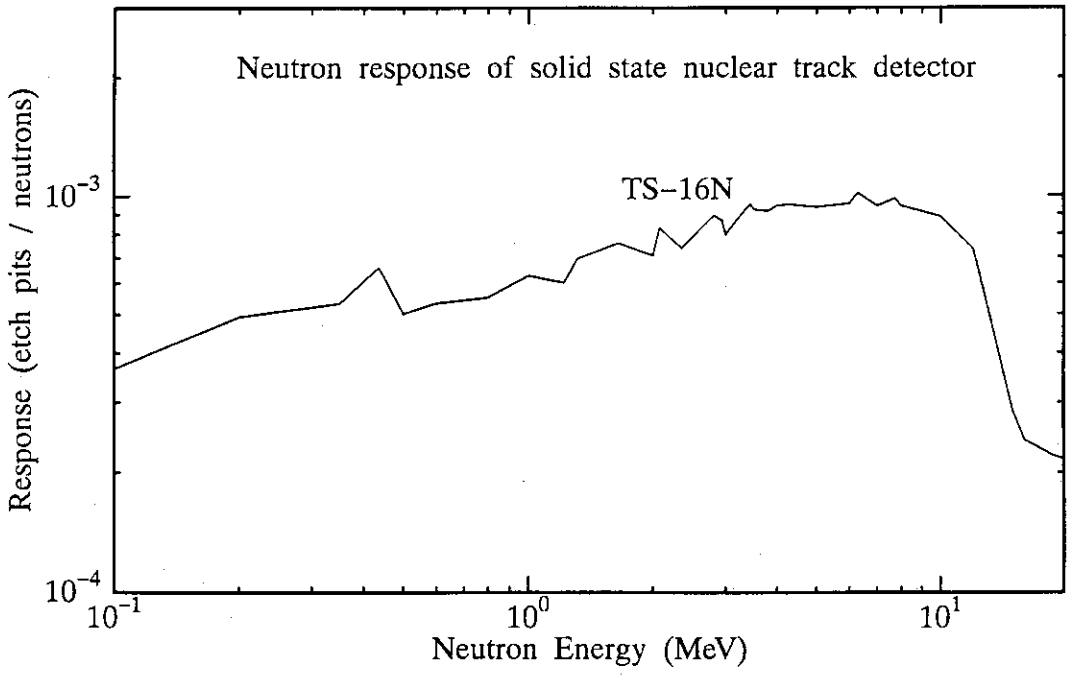

Fig. 8 Calculated neutron responses of solid state nuclear track detector (TS-16N) using the SSNRES code.

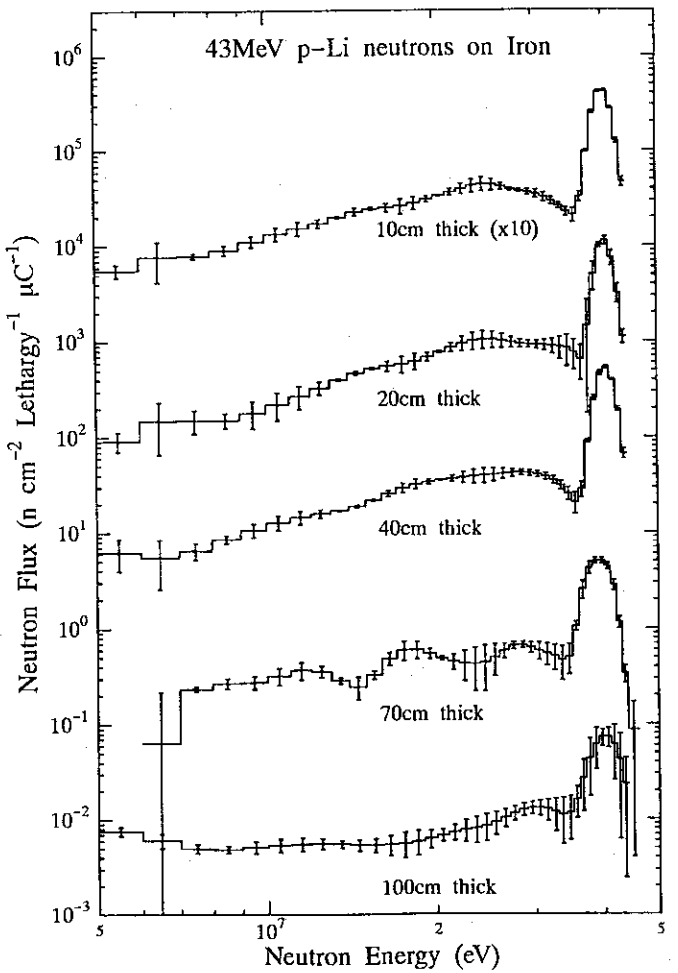

Fig. 9 Measured neutron spectra by the BC501A detector behind various thickness of iron on the beam axis for 43-MeV p-Li neutrons.

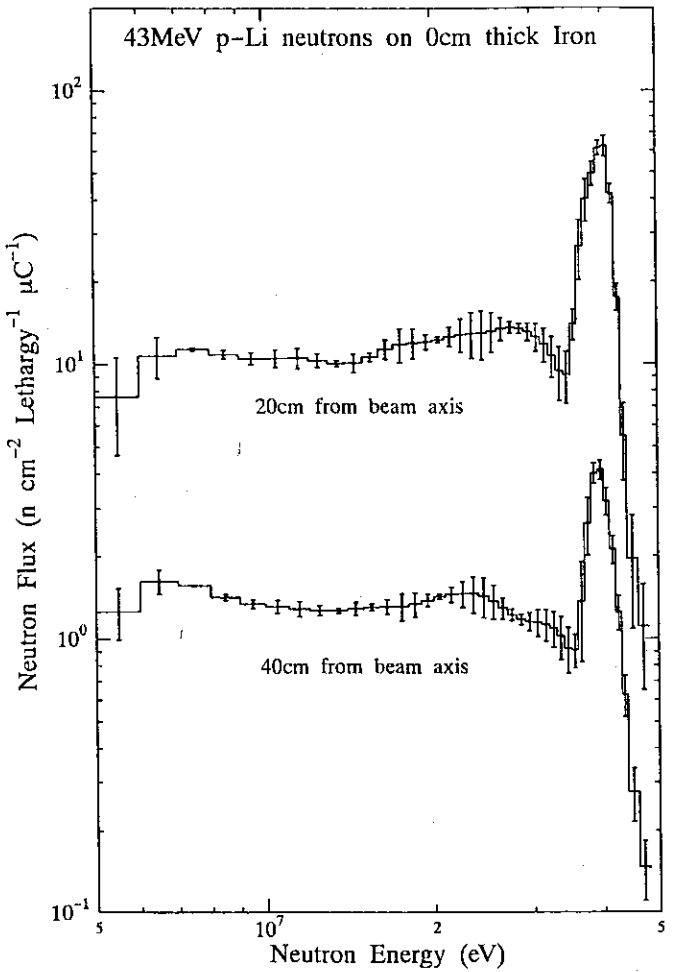

Fig. 10 Measured neutron spectra by the BC501A detector behind 0-cm thick iron at the positions of 20 and 40 cm from the beam axis for 43-MeV p-Li neutrons.

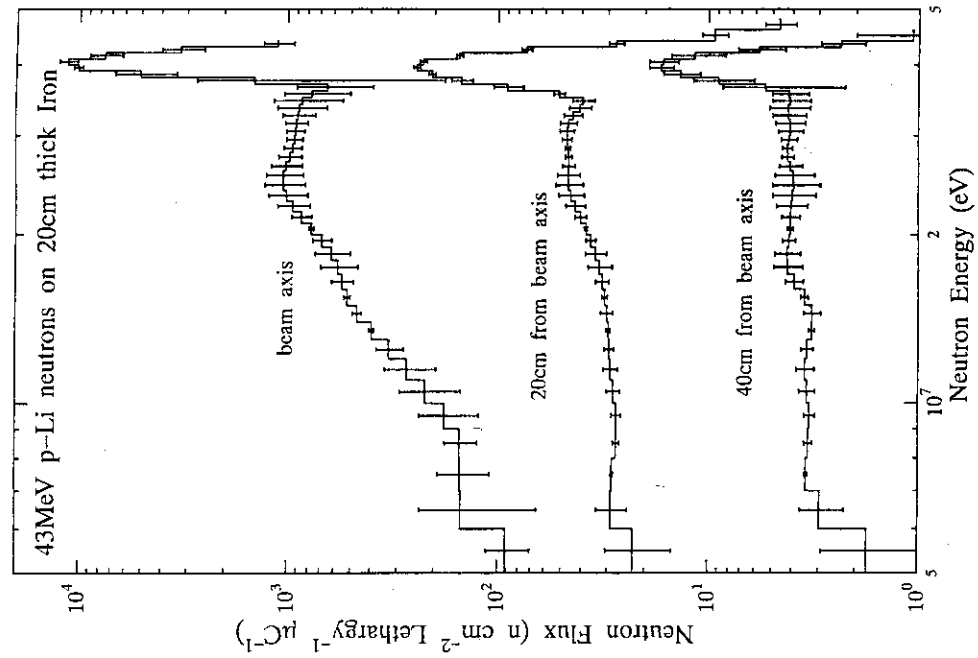

Fig. 12 Measured neutron spectra by the BC501A detector behind 20-cm thick iron on the beam axis and at the positions of 20 and 40 cm from the beam axis for 43-MeV p-Li neutrons.

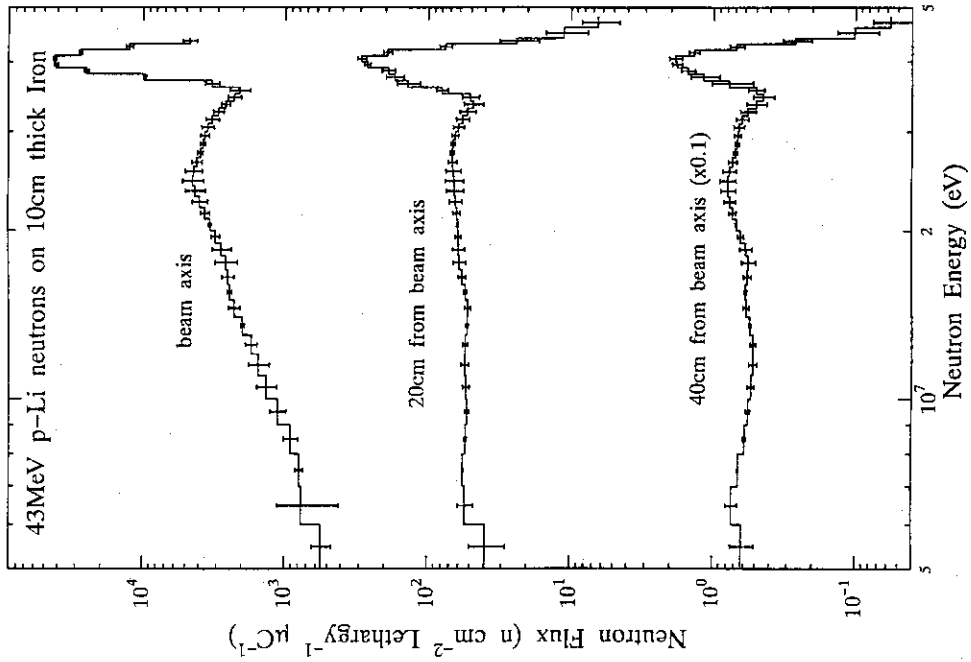

Fig. 11 Measured neutron spectra by the BC501A detector behind 10-cm thick iron on the beam axis and at the positions of 20 and 40 cm from the beam axis for 43-MeV p-Li neutrons.

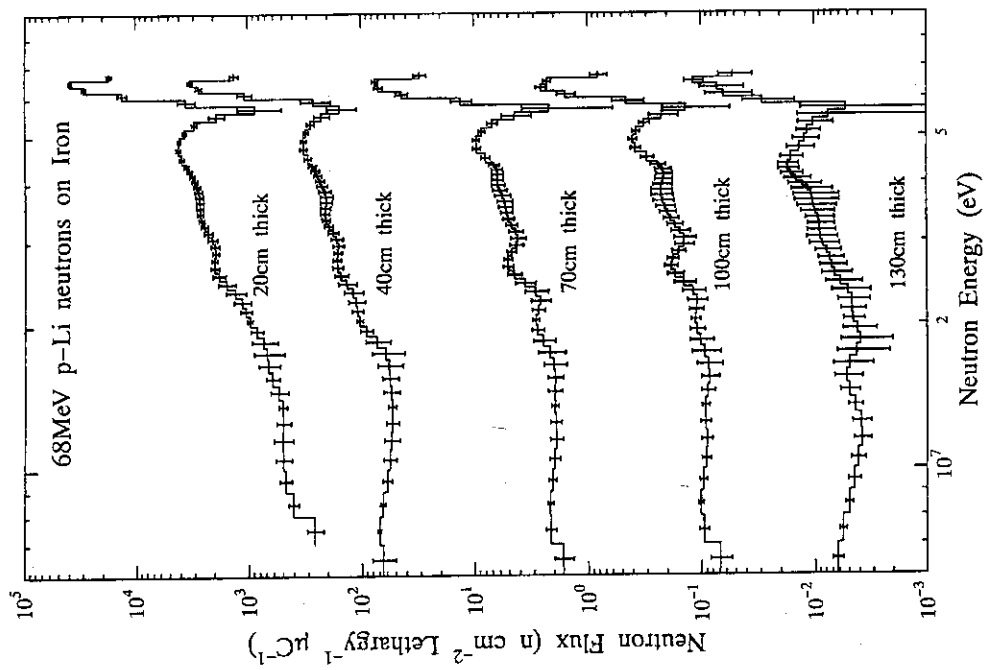

Fig. 14 Measured neutron spectra by the BC501A detector behind various thickness of iron on the beam axis for 68-MeV p-Li neutrons.

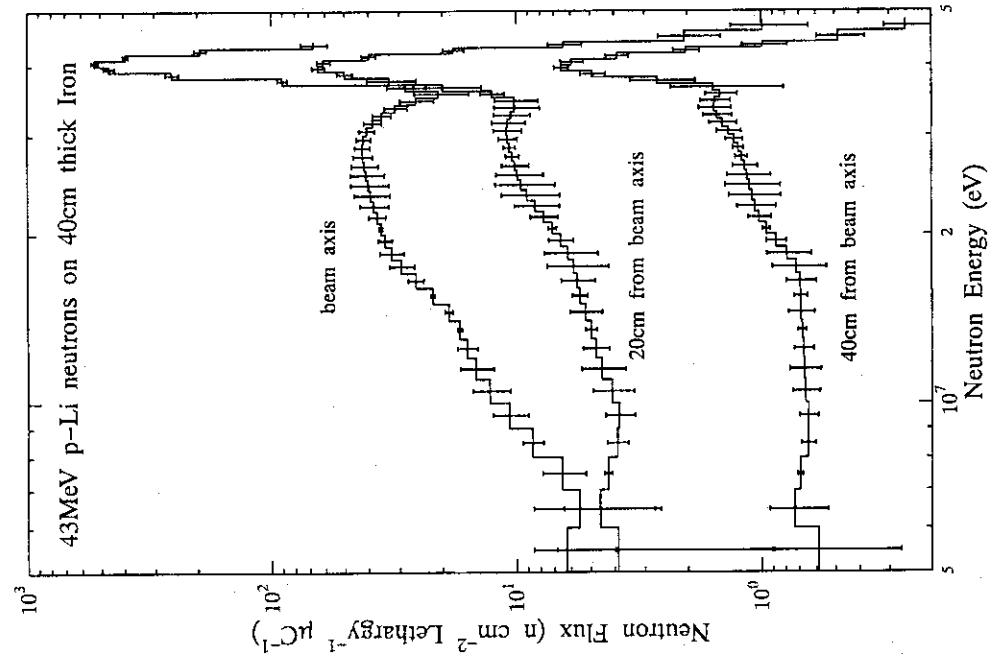

Fig. 13 Measured neutron spectra by the BC501A detector behind 40-cm thick iron on the beam axis and at the positions of 20 and 40 cm from the beam axis for 43-MeV p-Li neutrons.

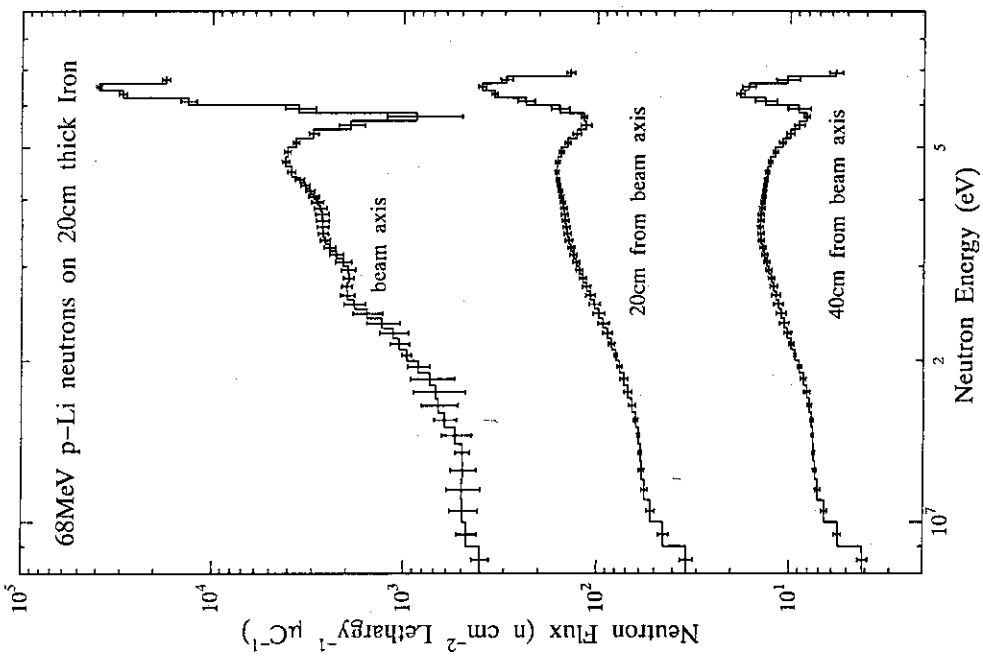

Fig. 16 Measured neutron spectra by the BC501A detector behind 20-cm thick iron on the beam axis and at the positions of 20 and 40 cm from the beam axis for 68-MeV p-Li neutrons.

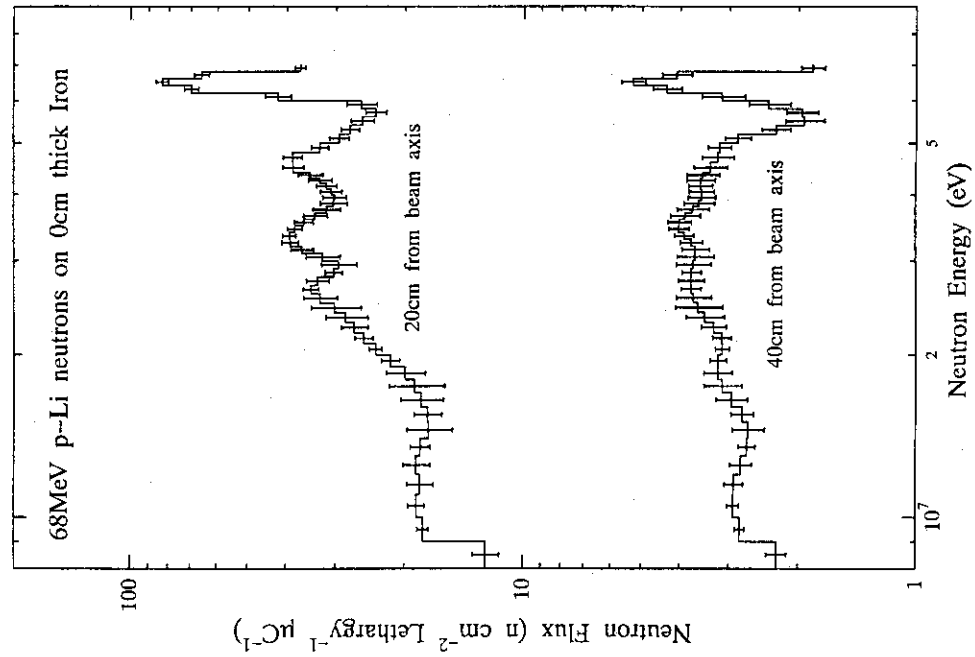

Fig. 15 Measured neutron spectra by the BC501A detector behind 0-cm thick iron at the positions of 20 and 40 cm from the beam axis for 68-MeV p-Li neutrons.

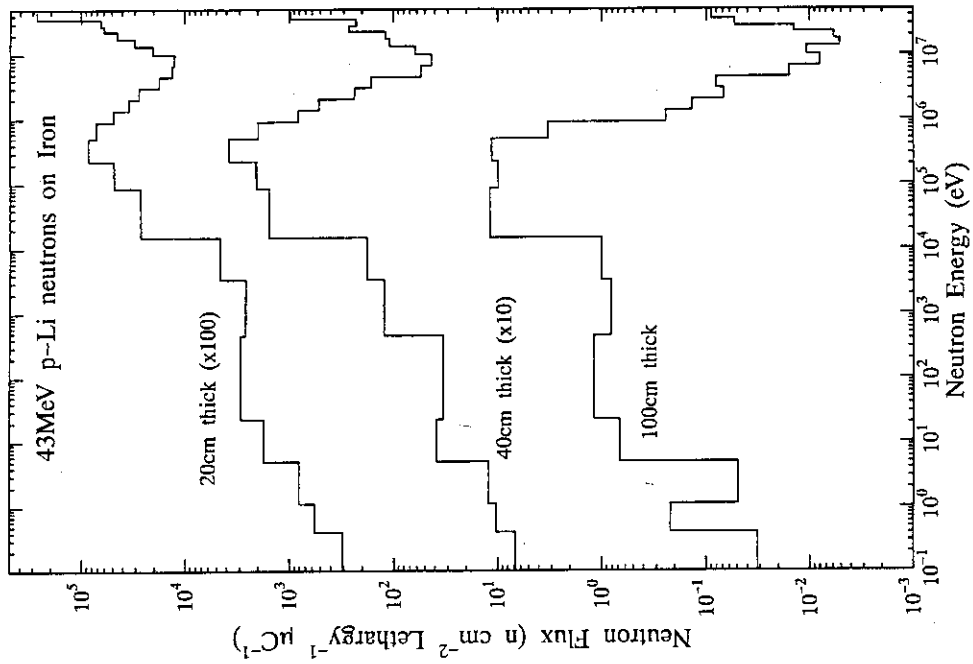

Fig. 18 Measured neutron spectra by the Bonner ball counter behind various thickness of iron on the beam axis for 43-MeV p-Li neutrons.

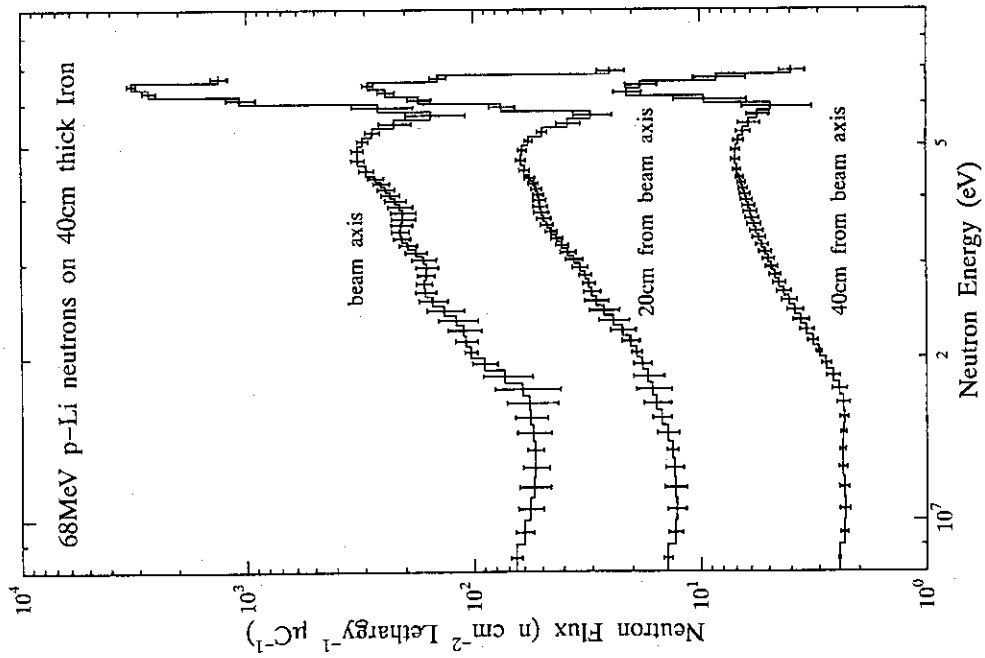

Fig. 17 Measured neutron spectra by the BC501A detector behind 40-cm thick iron on the beam axis and at the positions of 20 and 40 cm from the beam axis for 68-MeV p-Li neutrons.

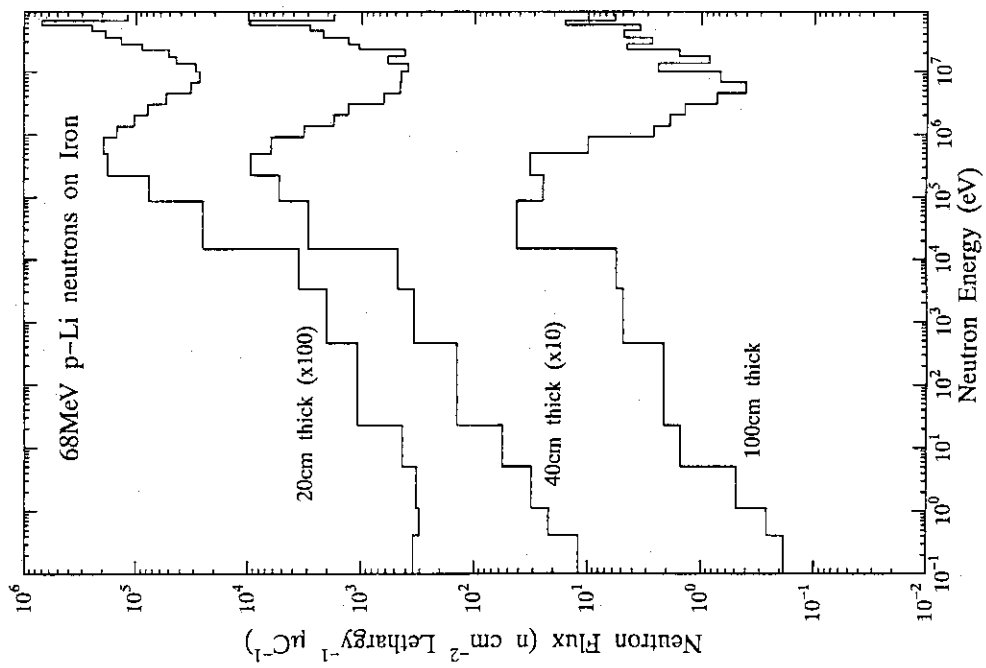

Fig. 19 Measured neutron spectra by the Bonner ball counter behind various thickness of iron on the beam axis for 68-MeV p-Li neutrons.

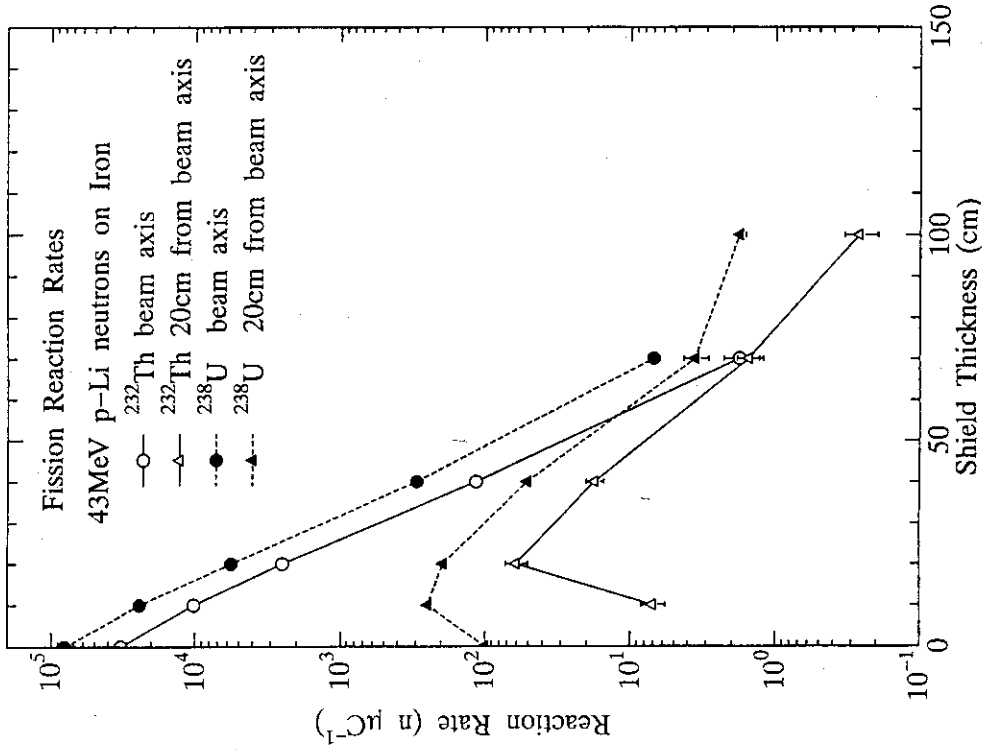

Fig. 20 Measured fission reaction rates of ^{238}U and ^{232}Th behind iron on the beam axis and at the position of 20 cm from the beam axis for 43-MeV p-Li neutrons.

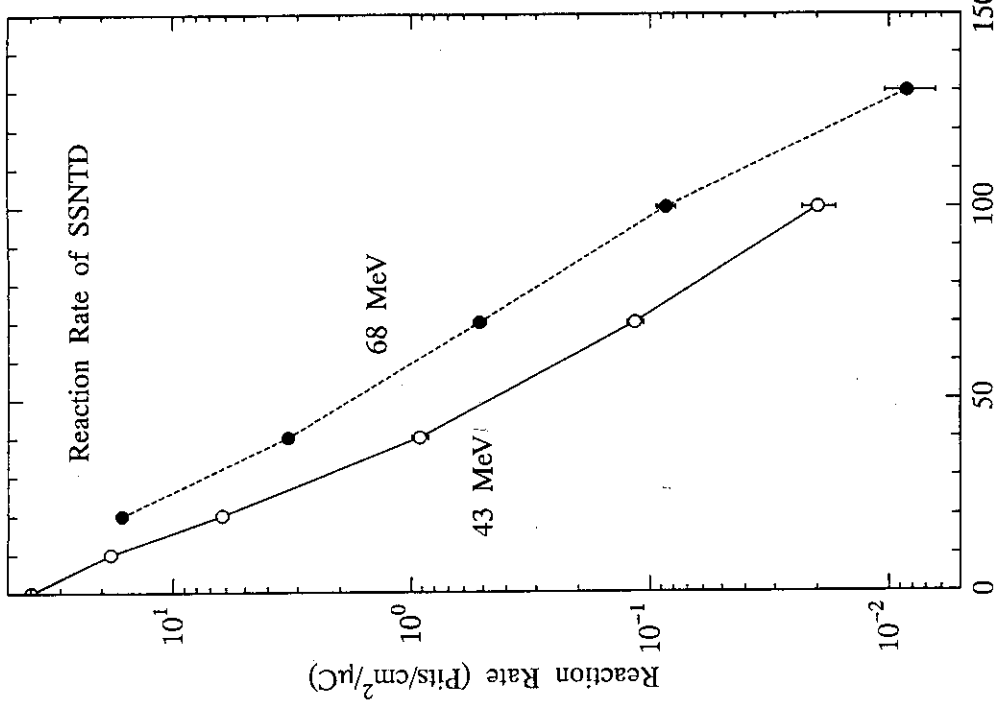

Fig. 22 Measured reaction rates of solid state nuclear track detector in the iron shield on the beam axis for 43-and 68-MeV p-Li neutrons.

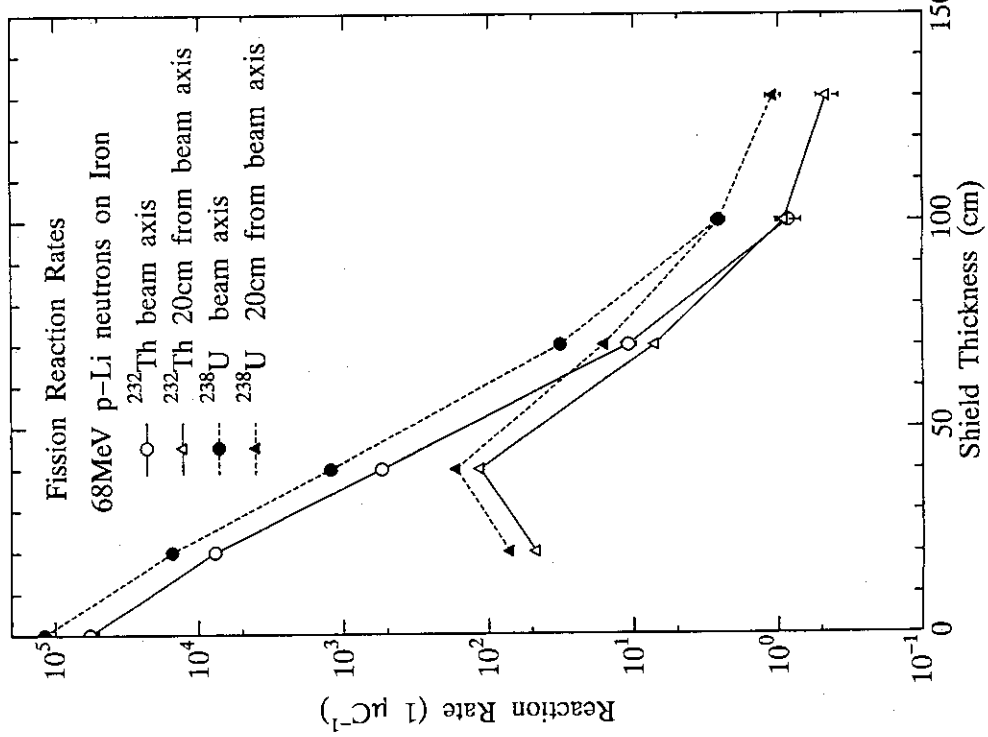

Fig. 21 Measured fission reaction rates of ^{238}U and ^{232}Th behind iron on the beam axis and at the position of 20 cm from the beam axis for 68-MeV p-Li neutrons.

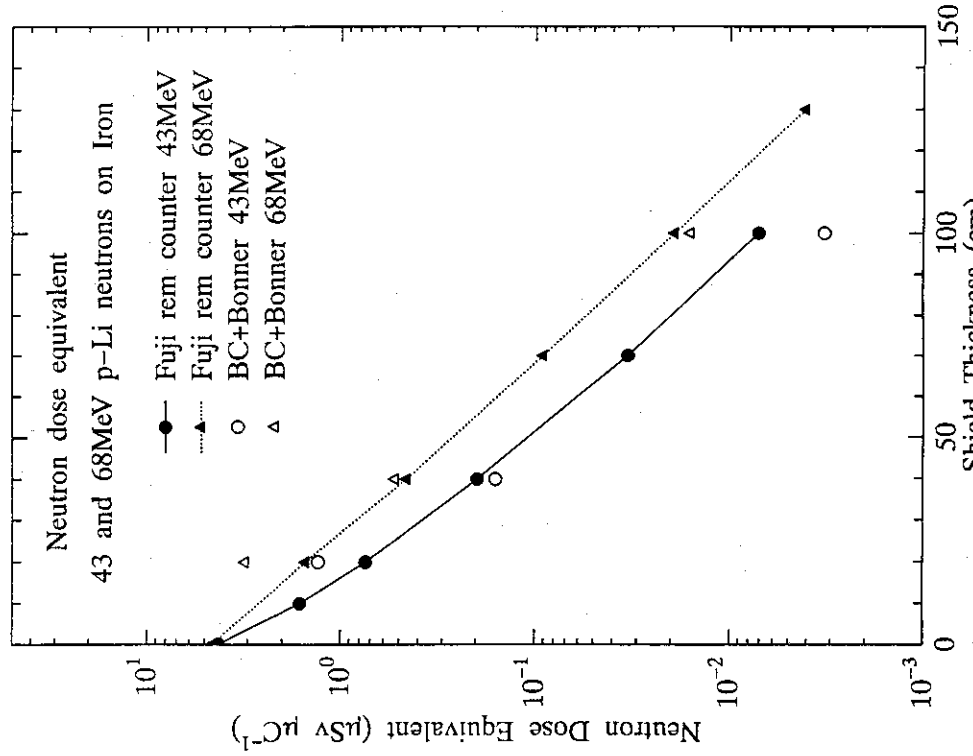

Fig. 23 Measured neutron does equivalent by the rem counter made by Fuji Co.Ltd. for 43-and 68-MeV p-Li neutrons. In this figure the measured neutron does equivalent by the BC501A and Bonner ball detectors are also shown.